THESIS APPROVAL

GRADUATE SCHOOL, KASETSART UNIVERSITY

Master of Science (Chemistry)
DEGREE

Chemistry
FIELD

Chemistry
DEPARTMENT

TITLE: Photoluminescent Study of Dy (III) and Mn (II) Doped $MgAl_2O_4$ Ceramics Prepared via One-pot Process

NAME: Mr. Watnatee Pullarp

THIS THESIS HAS BEEN ACCEPTED BY

THESIS ADVISOR
(Associate Professor SudjitSanguanruang, Ph.D.)

THESIS CO-ADVISOR
(Assistant Professor NattamonKoonsaeng, Ph.D.)

THESIS CO-ADVISOR
(Miss PornpunPornsinlapatip, Ph.D.)

DEPARTMENT HEAD
(Associate Professor WarapornParasuk, Dr.rer.nat.)

APPROVED BY THE GRADUATE SCHOOL ON _____

DEAN
(Associate Professor GunjanaTheeragool, D.Agr.)

THESIS

PHOTOLUMINESCENCE STUDY OF Dy(III) AND Mn(II) DOPED $MgAl_2O_4$ CERAMICS PREPARED VIA ONE-POT PROCESS

WATNATEE PULLARP

A Thesis Submitted in Partial Fulfillment of
the Requirements for the Degree of
Master of Science (Chemistry)
Graduate School, Kasetsart University
2014

Watnatee Pullarp 2014: Photoluminescent Study of Dy(III) and Mn(II) Doped $MgAl_2O_4$ Ceramics Prepared via One-pot Process. Master of Science (Chemistry), Major Field: Chemistry, Department of Chemistry. Thesis Advisor: Associate Professor Sudjit Sanguanruang, Ph.D. 68 pages.

A simple and less energy consuming method for preparing $MgAl_2O_4$ spinel and ion-doped $MgAl_2O_4$ ceramics was developed, adopting the process of oxide one-pot synthesis (OOPS) and stepwise calcination at low temperatures. The starting materials, *i.e.* Al_2O_3 , MgO, and triethanolamine were mixed at mole ratio of 1:1:3, using ethylene glycol as solvent. As for the doped ceramics, the dopant Dy(III) as $Dy(CH_3COO)_3$ or/and Mn(II) as $Mn(CH_3COO)_2$ was added in various mol% as desired. Four different types were prepared, *i.e.* undoped $MgAl_2O_4$, Dy(III)-doped, Mn(II)-doped, and Dy(III),Mn(II)-codoped $MgAl_2O_4$ ceramics. Brown polymer-like precursors were attained after heating the starting mixtures at 190 °C for 6 h. The precursors were then calcined in steps: 500 °C for 5 h, 750 °C for 5 h, and 850 °C for 2 h. The solid ceramics obtained were ground to powders. The XRD patterns indicated that the produced ceramics were not of pure spinel, but a solid solution of γ-Al_2O_3 and $MgAl_2O_4$. The compositions of the synthesized ceramics as determined by EDX, nonetheless, showed satisfactory doping yield of 99.26 ± 25.91 % at 95 %CL. The SEM images revealed the microstructure of the ceramics were mostly blocky particles in irregular shapes with hexagonal crystalline form appeared occasionally. A fiber-like structure also occurred in the codoped ceramics. Being excited at λ_{ex} 350.8 nm, the Dy(III)-doped ceramics emitted yellow fluorescence at λ_{em} 574.5 nm which was identified with the $^4F_{9/2}\rightarrow{}^6H_{13/2}$ transition of Dy(III). The Mn(II)-doped $MgAl_2O_4$, excited at λ_{ex} 302 nm, gave reddish-orange fluorescence at λ_{em} 658 nm corresponding to the $^4T_1\rightarrow{}^6A_1$ transition of Mn(II). It was found that the presence of Dy(III) in Dy(III),Mn(II)-codoped ceramics had intensified the 658-nm fluorescence of Mn(II) through a Dy(III)→Mn(II) energy transfer process.

_____ _____ __ / __ / __

Student's signature Thesis Advisor's signature

ACKNOWLEDGEMENTS

I wish to express my deep appreciation to my supervisor, Associate Professor Dr. Sudjit Sanguanruang, my co-supervisors, Assistant Professor Dr. Nattamon Koonsaeng, and Dr. Pornpun Pornsinlapatip, for their invaluable guidance, time and encouragement throughout the duration of my study and research.

I would like to thank the Kasetsart University Research and Development Institute (KURDI) for the financial support, the Department of Chemistry, Faculty of Science, Kasetsart University for all research facilities.

Last but not least, I am especially grateful to my parents for their consistent support morally and financially, their patient and understanding, their advice and encouragement, which made my graduate study possible. I would also like to thank all of my colleagues and friends for their unconditional friendship, their time and help during my graduate study.

Watnatee Pullarp

June, 2014

TABLE OF CONTENTS

Page

LIST OF TABLES

LIST OF FIGURES

LIST OF FIGURES (Continued)

Appendix Figure

LIST OF FIGURES (Continued)

LIST OF ABBREVIATIONS

PL	=	photoluminescence
RL	=	radioluminescence
XEL	=	x-ray-excited luminescence
XRF	=	x-ray fluorescence spectrometry
FTIR	=	fourier transform infrared spectroscopy
UV-vis DRS	=	uv-vis diffuse reflectance spectroscopy
MS	=	mass spectrometry
NMR	=	nuclear magnetic resonance spectrometry
ESR	=	electron spin resonance spectrometry
SEM	=	scanning electron microscopy
EDX	=	energy-dispersive x-ray spectroscopy
TEM	=	transmission electron microscopy
XRD	=	x-ray diffraction
JCPDS	=	joint committee on powder diffraction standards
g	=	gram
mol	=	mole
mmol	=	millimole
ppm	=	part per million
λ	=	wavelength
μm	=	micrometer
nm	=	nanometer
pm	=	picometer
h	=	hour
EG	=	ethylene glycol
TEA	=	triethanolamine
OOPS	=	oxide one-pot synthesis
CL	=	confidence limit
NR	=	non-radiative transition

PHOTOLUMINESCENCE STUDY OF Dy(III) AND Mn(II) DOPED $MgAl_2O_4$ CERAMICS PREPARED VIA ONE-POT PROCESS

INTRODUCTION

1. Photoluminescence

Photoluminescence (abbreviated as PL) is a process in which a substance absorbs photons (electromagnetic radiation) and then re-radiates photons. Quantum mechanically, this can be described as an excitation to a higher energy state and then return back to lower energy state accompanied by the emission of a photon. This is one of many forms of luminescence (light emission) and is distinguished by photoexcitation (excitation by photons), hence the prefix *photo*-. The period between absorption and emission is typically extremely short, in the order of 10 nanoseconds. Under special circumstances, however, this period can be extended into minutes or hours.

The simplest photoluminescent processes are *resonant radiations*, in which a photon of a particular wavelength is absorbed and an equivalent photon is immediately emitted. This process involves no significant internal energy transitions of the chemical substrate between absorption and emission and is extremely fast, of the order of 10 nanoseconds. More interesting processes occur when the chemical substrate undergoes internal energy transitions before re-emitting the energy from the absorption event. The most familiar such effect is *fluorescence*, which is also typically a fast process, but in which some of the original energy is dissipated so that the emitted light photons are of lower energy than those absorbed. The generated photon in this case is said to be red shifted, referring to the loss of energy as shown in *Jablonski diagram*, Figure 1.

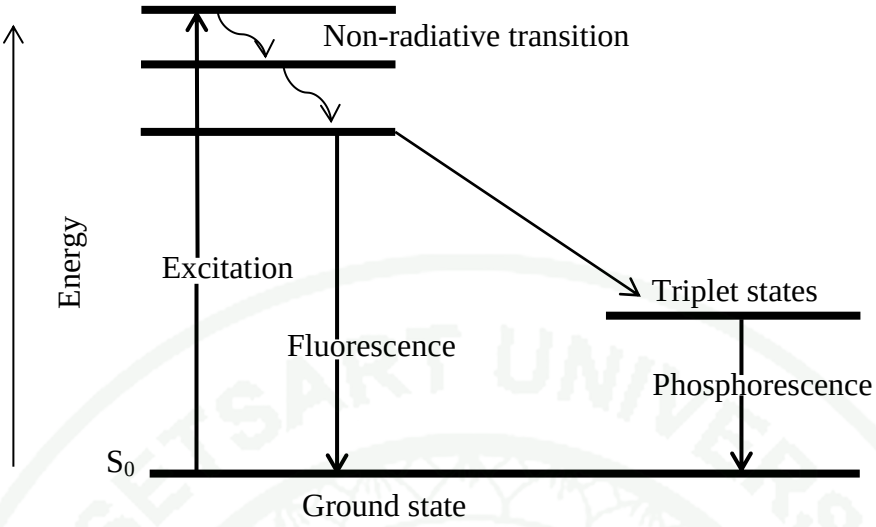

Figure 1 Jablonski diagram of fluorescence.

An even more specific form of photoluminescence is *phosphorescence*, in which the energy from absorbed photons undergoes intersystem crossing into a state of higher spin multiplicity, usually a triplet state. Once the energy is trapped in the triplet state, transition back to the lower singlet energy states is quantum mechanically forbidden, meaning that it happens much more slowly than other transitions. The result is a slow process of radiative transition back to the singlet state, sometimes lasting minutes or hours.

2. $MgAl_2O_4$ ceramics

The $MgAl_2O_4$ spinel belongs to the cubic space group O_h^7 (Fd3m) with eight formula units per unit cell, Figure 2. The first octant contains an Mg(II) ion at the center and has a tetrahedral coordination of O^{2-} ions with full T_d symmetry (A-site); the second octant has a six-fold distorted octahedral coordination of Al(III) ion belonging to the D_{3d} point group (B-site). In the recent years, several research groups have devoted significant efforts focusing on the persistent phosphorescence, the optically stimulated luminescence and photoluminescence, *etc*. By adding the rare-earth or transition elements in $MgAl_2O_4$ host, the luminescence is achievable (Vijay *et al*., 2007).

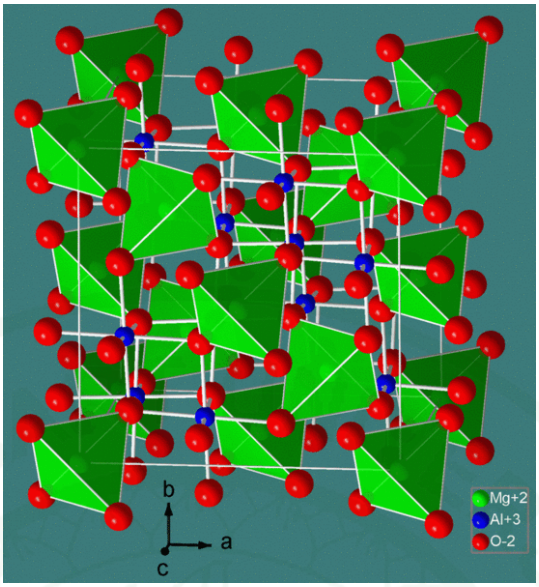

Figure 2 Crystal structure of spinel.

Ceramic lattices including phosphor materials can simply be prepared by conventional solid-state reaction (Gómez *et al*., 2004). However, the techniques involve high-temperature processing (some is >1250 °C) and long-period calcinations (can be up to 96 h). Several techniques were developed as alternative methods for the preparation of ceramic and phosphor materials, such as co-precipitate method (Dong *et al*., 2011), sol-gel method (Maia *et al*., 2008), floating-zone method (Hara *et al*., 2005), *etc*. In 2000, Laobuthee *et al*. proposed a simple, straight-forward oxide one-pot synthesis (OOPS) method. The OOPS was reported to be a low-temperature processing method, whereas the purity and homogeneity of the products were retained.

3. Doped $MgAl_2O_4$ ceramics

Rare-earth phosphors have been increasingly studied due to their preferable fluorescence properties, *e.g.* intense fluorescence, color-rendering index, energy efficiency, radiation stability, *etc.* Those rare-earth phosphors are found in various applications, such as luminous paints, display panels, emergency lighting, energy-saving fluorescent lamps, semiconductor light-emitting diodes, solid state lasers, optical amplifiers, *etc.* (Lai *et al*., 2008).

Dysprosium(III) is one of the most investigated ion as a potential white phosphor. Dy(III) emits two characteristic bands in blue (470-500 nm) and yellow (560-600 nm) regions which are corresponding to the $^4F_{9/2} \rightarrow {}^6H_{15/2}$ and $^4F_{9/2} \rightarrow {}^6H_{13/2}$ transitions, respectively. By adjusting the yellow-to-blue intensity ratio, a near-white emission can be obtained. Hence, it is possible to achieve the full color displays from the Dy(III)-activated luminescence materials. Dy(III) can be doped into different hosts, *e.g.* YPO_4:Dy(III), (Lai *et al*., 2008); YVO_4:Dy(III), (Omkaram *et al*., 2009); $MgAl_2O_4$:Dy(III), (Yu *et al*., 2002); $SrAl_2O_4$:Dy(III) and $CaAl_2O_4$:Dy(III), (Kat-sumata *et al*., 1998), *etc.*

The process of the generation of an emission of Dy(III) may be explained as the photon energy hυ causes the excitation of Dy(III). The excited electron of Dy(III) may relax to the $^4F_{9/2}$ excited state by non-radiative process and then followed by radiative transition from the excited state $^4F_{9/2} \rightarrow {}^6H_{13/2}$ emitting yellow light and $^4F_{9/2} \rightarrow {}^6H_{15/2}$ emitting blue light, shown in Figure 3.

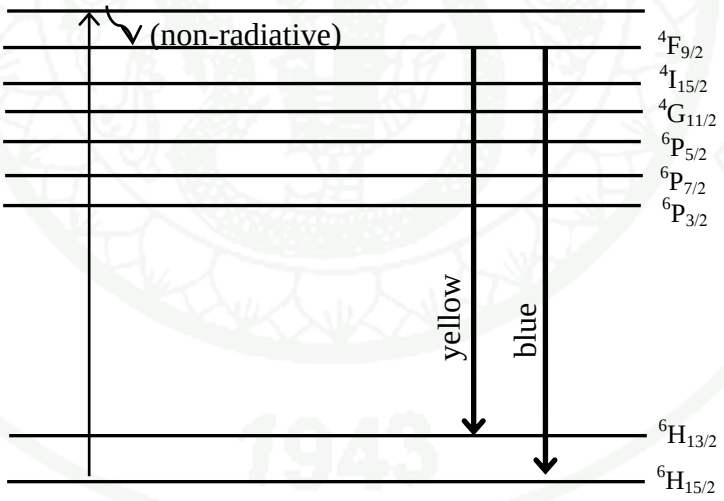

Figure 3 Emission mechanism in Dy(III) doped-powder phosphor.

Manganese(II)-doped luminescent materials are also of interest as candidates of red/orange phosphors with good red purity and high luminescence efficiency Mn(II) dopant does not affect the thermal stability and phase compositions of the parent host. and also found to be an efficient activator in several hosts. It needs, however, a

sensitizer, *e.g.* Eu(II), (Kawano *et al*., 2009). They show highly saturated color(s), high luminescence efficiency, and can be excited by all common excitation methods such as UV-irradiation, X-ray, and electric field.

The emission of Mn(II) is based on the $^4T_1(G) \rightarrow {}^6A_1(S)$ transition of Mn(II). The emission color varies from green to red, depending on the coordination number and the ligand field strength of Mn(II) (Tanabe *et al*., 1954). For examples, the luminescence of Zn_2SiO_4:Mn(II) is green, as Mn(II) has the coordination number of four with a weak ligand field (Sohn *et al.*, 1999). The orange luminescence is produced in the case of $Ca_5(PO_4)_3F$:Mn(II), where Mn(II) has the coordination number of six with a strong ligand field (Shinoya *et al.*, 1999). The process of generation of an emission as shown in Figure 4. After Mn(III) in host are excited. The e^- may relax to ^4E state which then relaxes non-radiatively to lower energy state such as $^4A_1$, ^4E and further to $^4T_1$ then radiative transitions to $^6A_1$ levels, causing orange/red emission

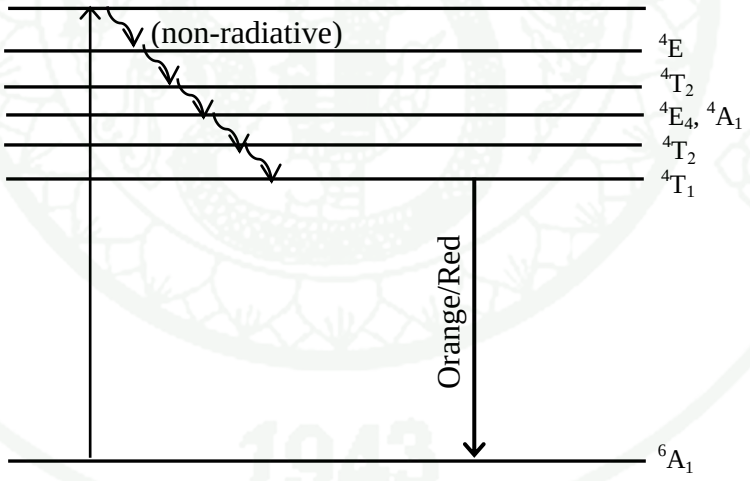

Figure 4 Emission mechanism in Mn(II) doped-powder phosphor.

4. Co-doped $MgAl_2O_4$ ceramics

The luminescence properties of co-activator compounds are of considerable interest. The main interest concerns the utilization of efficient energy transfer from one ion (sensitizer) to another ion (activator). These energy transfer phenomena lead to the

development of new and efficient photoluminescence materials. For example, CaF_2:Mn(II) does not fluorest under UV excitation, while CaF_2:Ce(III) emits a characteristic Ce(III) fluorescence (Lakshmanan, 1999). Furthermore, the com-bination of Ce(III) and Mn(II) in the CaF_2 lattice gives out brilliant Mn(II) fluores-cence in addition to that of Ce(III), due to the energy transfer from Ce(III) to Mn(II) ions.

The Dy(III), Mn(II) co-doped strontium aluminate phosphors are of the monoclinic structure (Karabulut *et al*., 2014). The characteristic luminescence of $^4F_{9/2} \rightarrow {}^6H_{15/2}$ (blue), $^4F_{9/2} \rightarrow {}^6H_{13/2}$ (yellow), $^4F_{9/2} \rightarrow {}^6H_{11/2}$ (red), and $^4F_{9/2} \rightarrow {}^6H_{9/2}$ (NIR) transitions of Dy(III) were detected in the emission spectra. The luminescence of Mn(II) co-doped $SrAl_2O_4$:Dy(III) phosphor particles exhibits a broad green/orange emission band ($^4T_1 \rightarrow {}^6A_1$ transition) with no transition of Dy(III). The energy transfer from Dy(III) to Mn(II) is realized through the exchange interaction.

The energy transfer process from Dy(III) to Mn(II) ions is described in the energy level scheme as shown in Figure 5. When the Dy(III) ions are excited to the excited state, they non-radiatively relax to $^4F_{9/2}$. The radiative transitions from $^4F_{9/2}$ of Dy(III) to $^6H_{13/2}$ levels give yellow emission. On the other hand, a part of the energy, observed in co-doped $SrAl_2O_4$:Dy(III), Mn(II), from the $^4F_{9/2}$ state can be directly transferred to ^4E of Mn(II), which then relaxes non-radiatively to $^4A_1$, ^4E and further to $^4T_1$ then radiative transitions to $^6A_1$ levels, causing orange/red emission. At 350 nm excitement, Mn^{2+} ions are also directly excited to ^4E. All these mechanisms lead to enhanced orange/red emission from co-doped $SrAl_2O_4$:Dy(III),Mn(II).

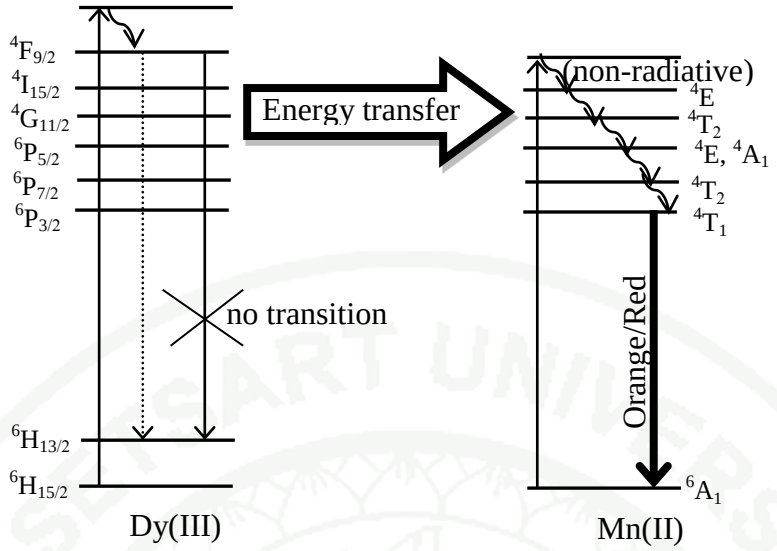

Figure 5 Schematic energy-level diagram showing energy transfer in co-doped $SrAl_2O_4$: Dy(III),Mn(II).

OBJECTIVES

1. To develop a method for the preparation of $MgAl_2O_4$ spinel and doped-$MgAl_2O_4$ ceramics via the process of oxide one-pot synthesis (OOPS) and stepwise calcination at low temperatures.

2. To synthesize phosphor-doped $MgAl_2O_4$ ceramics, *i.e.* Dy(III)-doped $MgAl_2O_4$, Mn(II)-doped $MgAl_2O_4$, and Dy(III),Mn(II)-codoped $MgAl_2O_4$, using the prior developed method.

3. To investigate the photoluminescence properties of the synthesized phosphor-doped $MgAl_2O_4$ ceramics.

LITERATURE REVIEW

The reviews aimed to compile the works done by previous researchers regarding to the preparation of magnesium aluminate ($MgAl_2O_4$) spinel and related phosphor materials. The studies on photoluminescence properties were also included.

$MgAl_2O_4$ spinel

In 1996, Waldner and coworkers reported a one-step reaction of $Al(OH)_3$ and MgO with triethanolamine in ethylene glycol that yielded a polymer-like precursor to spinel. From the spectroscopic studies (high-resolution MS, and ^{27}Al-solution NMR), the precursor appears to be a trimetallic double alkoxide consisting of two four-coordinate TEAA1 (alumatrane) moieties linked via a bridging TEA group that enfolds the Mg cation. Transformation of the precursor to pure spinel was reported to be a function of pyrolysis temperature and time. The product evolved upon pyrolysis at temperature 700 °C for 2 h in air to produce, apparently, a γ-Al_2O_3-$MgAl_2O_4$ solid solution. Upon pyrolysis at 1200 °C for 2 h, the precursor transformed to pure spinel which was confirmed by the XRD data.

In 2000, Laobuthee and colleagues prepared $MgAl_2O_4$ spinel powders using the oxide one-pot synthesis (OOPS) process. The mixture of Al_2O_3, MgO, TEA, and EG, placed in a 2-neck round-bottom flask, was heated at 190 °C with constant stirring for 6h. The reaction is as follows.

$$2Al(OH)_3 + MgO + 3TEA + EG \xrightarrow{190℃\,/-H_2O} \text{Spinel Precursor} \qquad (1)$$

The double alkoxide precursor of $MgAl_2O_4$ was then calcined under static air 1100 °C for 2h. Porous ceramic oxide bodies were produced from the spinel powders and characterized by SEM. Their electrical properties were studied using impedance spectroscopy over the frequency range from 10^{-2} to 10^5 Hz at different relative humidity (RH) levels over the range 4-90 %. The spinel pellets exhibited good

humidity sensitivity with a linear response of the logarithm of resistance with RH in the whole RH range tested. Hence, they can be used as humidity-sensing materials.

Barpanda *et al*. (2005) synthesized magnesium aluminate spinel powder using nitrate-citrate auto-ignition route with different ratios of nitrate and citrate solution. The obtained black ash was then calcined at different temperatures over the range of 650–1250 °C for 9 h. Phase evolution of the calcined powders as studied by XRD indicates the presence of structural disorder at low calcination temperatures, which can be transformed to an ordered structure at higher calcination temperatures. The order-disorder phase transition in the spinel sample was confirmed by Raman spectroscopy.

Doped phosphor host

In 1998, Katsumata and coworkers had grown long persistent phosphor crystals, *i.e.* $SrAl_2O_4$ doped with Eu and Dy; and $CaAl_2O_4$ doped with Eu and Nd, by a floating zone technique. The intensities and the persistent times of the phosphores-cences are found to depend on the growth atmosphere. $SrAl_2O_4$ crystals grown under H_2-Ar atmosphere and $CaAl_2O_4$ under the Ar exhibit strong and long persistent green (λ_{max} 520 nm) and blue (λ_{max} 450 nm) phosphorescence, respectively. The phosphor-escent spectra of the crystals are quite similar to those obtained from the sintered powders used in the luminous pigments. The persistent time of the $CaAl_2O_4$-crystal phosphorescence is similar to that obtained from the sintered powders. As for the $SrAl_2O_4$ crystals, the phosphorescent persistent time is shorter than that obtained from the sintered powders. The difference in the persistent time is due to the concentration of the Dy and/or Nd dopant added as auxiliary activators.

In 2004, Gómez and coworkers reported a comparative study of microwave and conventional processing of ceramic materials based particularly on $MgAl_2O_4$ sinters obtained from MgO and Al_2O_3 with 1 %wt of CaO as an additive, and Al_2O_3-$MgAl_2O_4$ composites. The microwave processing took place in air at 800 W and 2.45 GHz during 4.5 min, whereas the conventional processing was conducted in an electrical-resistance furnace, also in air, at 1400 °C for 96 h. The MgO:Al_2O_3 weight ratio

employed for the synthesis of $MgAl_2O_4$ was 1:2.45. According to the semi-quantitative X-ray diffraction analysis, approximately 90% of $MgAl_2O_4$ was produced by both processing methods. Scanning electron microscope (SEM) images revealed the microstructure of similar morphology from both methods; nevertheless the grain size was different. The Al_2O_3-$MgAl_2O_4$ composites were prepared via the two methods under the previous conditions, using the Al_2O_3:$MgAl_2O_4$ weight ratios of 9:1, 1:1, and 1:9. A heterogeneous microstructure was observed in the specimen processed by microwaves.

In 2008, Lai and coworkers employed the co-precipitation reaction soft chemistry method to prepare fine YPO_4:Dy(III) phosphor particles, calcined at 950 °C. The as-prepared samples were characterized by XRD, transmission electron micrograph (TEM) and photoluminescence (PL) spectroscopy. The obtained YPO_4 nanocrystals appeared to be spherical with some agglomeration, and their sizes ranged from 20 to 40 nm. The characteristic transitions of Dy(III) due to $^4F_{9/2} \rightarrow {}^6H_{15/2}$ (blue) and $^4F_{9/2} \rightarrow {}^6H_{13/2}$ (yellow) were detected in the emission spectra.

In 2009, Omkaram and colleague synthesized trivalent dysprosium activated magnesium aluminate phosphors by high-temperature solid-state reaction method. The obtained $MgAl_2O_4$:Dy(III) phosphors have good crystallinity, spherical morphology with the sizes ranged from 120 to 140 nm. Strong blue emission was obtained under an excitation of 258 nm. The emission spectrum of the Dy(III) doped-$MgAl_2O_4$ phosphor consists of two emission bands: blue and yellow. The emission intensity of the blue band is stronger than that of the yellow.

In 2002, Yu and coworkers fabricated the nanocrystalline YVO_4:A (where A = Eu(III), Dy(III), Sm(III), Er(III)) phosphor films and their patterning by a Pechini sol-gel process combined with soft lithography. The XRD results indicated that the films began to crystallize at 400 °C and the crystallinity increased with the increase of annealing temperatures. The transparent non-patterned phosphor films were uniform and crack-free, and mainly consisted of grains with an average size of 90 nm. Patterned gel and crystalline phosphor film bands with different widths (5-60 μm) were

obtained. Significant shrinkage and a few defects were observed in the patterned films during the heat treatment process. The doped rare-earth ions (A) displayed their characteristic emission in the crystalline YVO_4 phosphor films owing to the efficient energy transfer from the vanadate group to the rare-earth ions. The Sm(III) and Er(III) ions also showed up conversion luminescence in an YVO_4 film host. The lifetime and the PL intensity of the rare-earth ions increased with increasing annealing temperature from 400 to 800 °C. The optimum concentration of Eu(III) was determined to be 7 mol %, and those of Dy(III), Sm(III), and Er(III) were 2 mol % of Y(III) in the YVO_4 films, respectively.

In 2008, Maia and coworkers prepared $MgAl_2O_4$:Eu,Dy nanoparticles by citrate sol-gel method, and thermally treated at 600, 700, 800 and 900 °C. The IR spectra of the phosphors showed the bands around 700 and 520 cm^{-1} corresponding to the AlO_6 groups. The XRD patterns present sharp reflections of samples heated from 700 to 900 °C indicating the $MgAl_2O_4$ spinel phase. The grain size observed by TEM were in the range of 20-30 nm. The trivalent europium ion is partially reduced to the divalent state at 700 and 800 °C. A broaden band in the emission spectra of the phosphors was found at 480 nm which was assigned to the $4f^6 5d \rightarrow 4f^7$ ($^8S_{7/2}$) transition of Eu(II) ion overlapped with the $^4F_{9/2} \rightarrow {}^6H_{15/2}$ transition of the Dy(III) ion. The $^4F_{9/2} \rightarrow {}^6H_{13/2}$ transition of Dy(III) ion (at 579 nm) was also overlapped with the $^5D_0 \rightarrow {}^7F_0$ (578 nm) and $^5D_0 \rightarrow {}^7F_1$ (595 nm) transitions of the Eu(III) ion. The excitation spectra of the sample heated at 900 °C monitoring the excitation at 615 nm of $^5D_0 \rightarrow {}^7F_2$ transition of Eu(III) ion exhibit a broad band at ~280 nm, assigned to the $O \rightarrow Eu^{3+}$ ligand-to-metal charge-transfer states (LMCT). The samples exhibit a green persistent luminescence after exposing to the UV radiation. The chromaticity coordinates were obtained from the luminescence emission spectrum.

Vijay *et al*. (2007) prepared the $MgAl_2O_4$:Mn phosphors at 500 °C by combustion route. The powder XRD indicated the presence of mono-$MgAl_2O_4$ phase. The SEM images showed that the powder particle crystallites were mostly angular. The presence of AlO_6 group which made up the $MgAl_2O_4$ spinel was confirmed by Fourier transform infrared spectrometry. The photoluminescence studies showed the

green and red emissions indicating two independent luminescence channels in this phosphor. The green emission at 518nm is due to the $^4T_1 \rightarrow {}^6A_1$ transition of Mn(II) ions. The emission at 650 nm is due to the charge-transfer de-excitation associated with the Mn ion.

Zhihua *et al*. (2005) developed an efficient way to search a host for UV phosphor from UV-nonlinear-optical (NLO) materials. $Na_3La_2(BO_3)_3$ or NLBO, a promising NLO material with a broad transparency range and high damage threshold, was adopted as a host material. The lanthanide ions (Tb(III) and Eu(III))-doped NLBO phosphors were synthesized by solid-state reaction. The luminescent properties of the Ln-doped (Ln = Tb(III), Eu(III)) sodium lanthanum borate were investigated under the UV excitation. The emission spectrum was employed to probe the local environments of Eu(III) ions in the NLBO crystal. For red phosphor NLBO:Eu, a dominating emission peak is found at 613 nm which is attributed to the $^5D_0 \rightarrow {}^7F_2$ transition of Eu(III). The luminescence indicates that the local symmetry of Eu(III) in the NLBO lattice has no inversion center. The optimum concentration of Eu(III) in NLBO:Eu(III) under UV excitation with 395nm wavelength is about 30 mol%. The green phosphor, NLBO:Tb, emitted bright green light of 543 nm when being excited at 252 nm. The maximum concentration of Tb(III) in the NLBO:Tb, measured from the concentration quenching curve, was about 20%. The luminescence mechanism of the Ln-doped NLBO was analyzed.

Fang *et al*. (2009) synthesized the submicrometer crystalline $CaMO_4$:RE(III) (M = W, Mo; RE = Eu, Tb) phosphors of a sheelite structure via the hydrothermal process. The phosphors were characterized by powder XRD, FTIR, X-ray-excited luminescence (XEL), UV-vis diffuse reflectance spectroscopy (UV-vis DRS) and SEM, respectively. The XRD patterns indicated the same structure of $CaWO_4$ and $CaMoO_4$. The SEM images showed the particles aggregation with the increase of temperature. The optimal hydrothermal temperature was found to be 120 °C. The bands ranging from 380 to 510 nm in the XEL spectra of $CaWO_4$:Eu(III) can be attributed to the charge transfer state from the excited 2*p* orbitals of O^{2-} to the empty orbitals of the central W(VI) of the tungstate groups. The comparison between the photoluminescent

lifetime and the quantum efficiency of the two phosphors was also investigated. The $CaMoO_4$:Eu(III) phosphor has three main emission peaks at 592.8, 615, and 702.4 nm, which correspond to the $^5D_0$–$^7F_1$, $^5D_0$–$^7F_2$, and $^5D_0$–$^7F_4$ transitions of Eu(III) ion. The electric dipole transition of $^5D_0$–$^7F_2$ is more prominent compared to the magnetic dipole transition of $^5D_0$–$^7F_1$ at 592.8 nm.

Yan *et al*. (1998) prepared ternary complexes of europium and terbium with *p*-aminobenzoic acid and 1,10-phenanthroline, (Eu(*p*-ABA)$_3$.phen.2H_2O and Tb(*p*-ABA)$_3$.phen.2H_2O, where *p*-HABA = *p*-aminobenzoic acid and phen = 1,10-phenanthroline) and introduced the complexes into a silica matrix by sol-gel method. The luminescence behavior of the complexes in silica gels was studied in comparison with the corresponding solid-state complexes by means of emission, excitation spectra, and lifetimes. Within the range of dopant concentrations, the luminescence intensities of rare-earth complexes in silica gel increase with the increasing of their dopant concentration. The lifetimes of rare-earth ions (Eu(III) and Tb(III)) in silica gel doped with europium and terbium complexes become longer than those in pure complexes. Very small amounts of rare-earth complexes doped in silica gel matrix can exhibit excellent luminescence properties. The luminescence properties of the Eu- and Tb-complexes with *p*-aminobenzoic acid and 1,10-phenanthroline incorporated into silica gel with different dopant concentrations can be seen that the luminescence intensities of Tb(*p*-ABA)$_3$.phen.2H_2O and Eu(*p*-ABA)$_3$.phen.2H_2O doped in silica matrix increase with the increase of corresponding dopant concentrations of them.

Yong *et al*. (1996) studied the luminescence of SrB_4O_7:*x*Eu,*y*Tb phosphors. The emission spectra of Eu(II), Eu(III) and Tb(III) ions in the phosphors were observed. The relative intensity of the emission of Eu(II) ion in the same matrix were found to increase when Tb(III) was incorporated in the SrB_4O_7:Eu phosphor. The valence state of europium is influenced by the presence of terbium. The Eu(III) ion with a $4f^6$ configuration tends to gain an electron whilst the Tb(III) ion ($4f^8$ configuration) is likely to lose an electron in order to attain the stable state of half-filled $4f^7$ electronic configuration. When the Eu(III) and Tb(III) ions are co-doped in the SrB_4O_7 matrix, an electron can be easily transferred from Tb(III) to Eu(III).

Guanghuan *et al*. (2010) synthesized the red phosphors $CaAl_2O_4$:EuIII),R(I) (R = Li, Na, K) by solid state reaction method. The XRD and PL were employed to characterize their structural and luminescent properties. The optimal sintering temperature and sintering time were found at 1200 °C and 4h, respectively. The optimal concentration of doped Eu(III) was 3 mol%. Under the ultraviolet excitation at 254 nm, the samples gave red luminescence which probably attributed to the transitions from $^5D_0$ excited state to ^7F_J (J = 0-4) ground states of Eu(III) ions. The feature and the high intensity of the hypersensitive transition $^5D_0 \rightarrow {}^7F_2$ indicated that Eu(III) preferred to occupy a low symmetry site. The incorporation of alkali metal ions greatly enhanced the luminescence intensity, probably due to the influence of the charge compensation of alkali metal ions.

Gedam *et al.* (2007) synthesized halosulphate phosphors, *i.e.* Ce(III)-doped-$KMgSO_4$; $KMgSO_4$Cl:Ce(III),Dy(III); and $KMgSO_4$Cl:Ce(III),Mn(II) by wet chemical method. The phosphors were characterized by the powder XRD and PL. The effects of Dy(III) and Mn(II) co-doping on the photoluminescence characteristics of $KMgSO_4$Cl:Ce phosphor were studied. The energy transfer from Ce(III)→Dy(III) and Ce(III)→Mn(II) results in the increase in PL peak intensity suggesting that Ce(III) plays an important role in PL emission in the present matrix. The PL emission spectra exhibited two peaks (482 and 571 nm) and a single peak (564 nm), which could be attributed to the Ce(III)→Dy(III) and Ce(III)→Mn(II) emissions, respectively.

In 2004, Tomita and coworkers observed two independent luminescence channels from the manganese-doped spinel $MgAl_2O_4$:Mn. The luminescence at ~520 nm was assigned to the transition from the lowest electronic excited state $^4T_1$ to the ground state $^6A_1$ of Mn(II) ($3d^5$) ion by analyzing the excitation spectrum and the electron spin resonance (ESR) measurement. The emission at 650 nm, triggered by the band edge excitation, was assigned similarly to the charge-transfer process associated with the manganese ion.

Tong *et al.* (2012) reported the synthesis of Mn-doped ZnO with intra-manganese luminescence in a thermal evaporation system without catalysts or gas flow.

The as-grown products are nanorods of several micrometers in length and about 100 nm in diameter. The microstructure analysis reveals that the obtained Mn-doped ZnO nanorods are of high crystallinity and along the [0001] direction growth. The PL spectrum of the Mn-doped ZnO nanorods displays a strong yellow/orange emission at 575 nm from the $^4T_1(G) \rightarrow {}^6A_1(S)$ transition of internal Mn(II).

Zhang (2013) and his coworkers studied the photoluminescence properties of Dy(III)-activated $Gd(BO_2)_3$ phosphors by means of fluorescence dynamics excited by pulsed laser light (k = 266 nm). The energy transfer from Gd(III) to Dy(III) and the concentration quenching of the Dy(III) luminescence were investigated. The energy transfer from Gd(III) to Dy(III) was confirmed by the PL spectra and the decay curves which exhibited the build-up and the decay processes of Dy(III) $^4F_{9/2}$–$^6H_{13/2}$ transition. The rise time becomes shorter as the Dy(III) concentration increases. The theoretical luminescence decay curves of $(Gd_{1-x}Dy_x)(BO_2)_3$ samples agree well with the experimental observations. The concentration quenching of the Dy(III) ion emission can be ascribed to the resonant cross-relaxation. The interaction between the Dy(III) ions is probably of the electric dipole-dipole type, suggested through the data fitting with Inokuti-Hirayama (I-H) model. The energy transfer parameters and the critical distance for the transfer processes were given.

Karabulut and coworkers (2014) prepared the strontium aluminate co-doped with dysprosium and manganese by a solid-state reaction at temperatures at 1600 °C under the H_2-Ar (15:85 %) atmosphere. The Dy,Mn co-doped strontium aluminate phosphors are of the monoclinic structure with the lattice parameters: a ~8.440 Å, b ~8.821 Å, and c ~5.157 Å. The characteristic luminescence of $^4F_{9/2} \rightarrow {}^6H_{15/2}$ (blue), $^4F_{9/2} \rightarrow {}^6H_{13/2}$ (yellow), $^4F_{9/2} \rightarrow {}^6H_{11/2}$ (red), and $^4F_{9/2} \rightarrow {}^6H_{9/2}$ (NIR) transitions of Dy(III) from different luminescence techniques (radioluminescence, photolumines-cence and cathodoluminescence) were detected in the emission spectra at room temperature. The luminescence of Mn(II) co-doped $SrAl_2O_4$:Dy(III) phosphor particles exhibits a broad green/orange emission band ($^4T_1 \rightarrow {}^6A_1$ transition) under different excitation sources. Multiple emission lines observed in the emission spectra are due to the crystal field splitting of the ground state of the emitting ions.

Caldino *et al.* (2012) investigated the photoluminescence of zinc metaphosphate glasses activated by Dy(III), Ce(III)/Dy(III) and Ce(III)/Dy(III)/Mn(II) ions. Non-radiative energy transfers from Ce(III) to Dy(III) and Ce(III) to Mn(II) are observed upon 280 nm excitation. The non-radiative nature of these transfers is inferred from the increase in the decay rate of the Ce(III) emission when the glasses are co-doped with Dy(III) or Dy(III)/Mn(II). It was found that zinc metaphosphate glasses could emit either cold or warm white light when they were doped with Ce(III)/Dy(III) or Ce(III)/Dy(III)/Mn(II) and λ_{ex} at 280 nm (the λ_{em} peak of AlGaN-based LEDs). The CIE 1931 chromaticity coordinates and color temperature were (0.34, 0.35) and 5250 K for the cold light, and (0.47, 0.43) and 2700 K for the warm light.

Lakshminarayana and Wondraczek (2011) investigated the efficiency of Tb(III) as sensitizer for red photoemission from Mn(II)-centers in ZnO-B_2O_3-Al_2O_3-Si_2O-Na_2O-SrO glasses and the corresponding gahnite glass ceramics. In comparison to singly or co-doped glasses, the glass ceramics exhibit significantly increased emission intensity. Structural considerations, ESR, and dynamic luminescence spectroscopy indicate the partial incorporation of Mn(II) (on the octahedral Zn(II)-sites) as well as Tb(III) into the crystalline phase. The interionic distance and charge transfer probability between both species depend on the crystallization conditions; hence, enabling the control of energy transfer process, and in turn, the tenability of the photoemission color by the simultaneous emission from Tb(III) and Mn(II) centers. The concentration quenching in the Mn(II)-singly doped materials was found at a critical dopant concentration of about 1.0 mol%. The energy transfer process was studied by both dynamic and static luminescence spectroscopy. Spectroscopic results suggested the studied materials could be used as single- or dual-mode emitting phosphor for luminescent lighting.

Ayvacikli *et al.* (2013) synthesized a new phosphor $SrAl_2O_4$:Mn(II) co-doped with Nd(III) by a traditional solid-state reaction method. The influence of transition metal and rare earth doping on crystal structure and their luminescence properties were investigated by XRD, Raman scattering, PL, and Radioluminescence (RL) techniques. The diffraction patterns revealed a major phase characteristic of the monoclinic

$SrAl_2O_4$ compound. Small amounts of the dopants $MnCO_3$ and Nd_2O_3 had almost no effect on the crystalline phase composition. The characteristic absorption bands of Nd(III) 4f–4f transitions in the spectra can be assigned to the transitions from the ground state $^4I_{9/2}$ to the excited states. The luminescence of Mn(II)-activated $SrAl_2O_4$ exhibits a broad green emission band under different excitation sources. The emitted radiations, observed in PL and RL spectra, were dominated by the visible 560 nm, and the peaks at 870, 1057, and 1335 nm in the NIR region as a result of $^4I_{9/2} \rightarrow {}^4G_{7/2}$ and $^4F_{3/2} \rightarrow {}^4I_J$ (J = 9/2, 11/2 and 13/2) transitions of Nd(III) ions, respectively.

Ummartyotin and coworkers (2012) prepared ZnS and metal (Mn, Cu)-doped-ZnS by wet chemical synthetic route. The FTIR and XRD methods were used to determine the chemical bonding and crystal structure, respectively. It was found that small amount of metal dopant (Mn, Cu) could be completely substituted into the ZnS lattice, leading to the transfer of the luminescent centre. The existence of the metal-doped ZnS was confirmed by X-ray fluorescence spectrometry (XRF). The SEM images revealed the blocky particles with irregular sharpness. The PL and laser confocal microscopy showed that the phosphors ZnS, Mn-doped-ZnS, and Cu-doped-ZnS generated blue, yellow and green color, respectively.

MATERIALS AND METHODS

Materials

Chemical reagents

The following reagents used for the synthesis of the ceramics in this work were purchased from commercial sources. They were kept in a desiccator until use without further purification.

Magnesium oxide; MgO, (Carlo Erba)

Aluminum hydroxide, hydrate; $Al(OH)_3.xH_2O$, 63.18% Al_2O_3 (Aldrich)

Dysprosium(III) acetate, hydrate; $Dy(C_2H_3O_2)_3.xH_2O$, 99.9% (Aldrich)

Manganese(II) acetate, tetrahydrate; $Mn(C_2H_3O_2)_2.4H_2O$ (Univar)

Ethylene glycol (EG); $HOCH_2CH_2OH$ (Carlo Erba)

Triethanolamine (TEA); $N(CH_2CH_2OH)_3$ (Asia Pacific Specialty)

Instrument

X-ray diffraction spectrometer; Jeol™, model JDX-3530.

Scanning electron microscope equipped with EDX; Phillips™, model XL30.

Spectrofluorometer; PerkinElmer™, model LS55.

Furnace; Hope Vally™, model LFT 12/75/610.

Methods

1. Preparation of ceramics

1.1 Preparation of undoped-ceramic $MgAl_2O_4$

Magnesium aluminate was prepared by the oxide one-pot synthesis (OOPS) process as followed: 50 mmol of $Al(OH)_3.xH_2O$ (63.18 % as Al_2O_3, 8.069 g), 50 mmol of MgO (2.016 g), 150 mmol of TEA (20 ml), and 100 ml of EG were placed in a 2-neck, round-bottom flask. The equipment is setup as shown in Figure 6. The mixture was heated at 190 °C with constant stirring for 6 h.

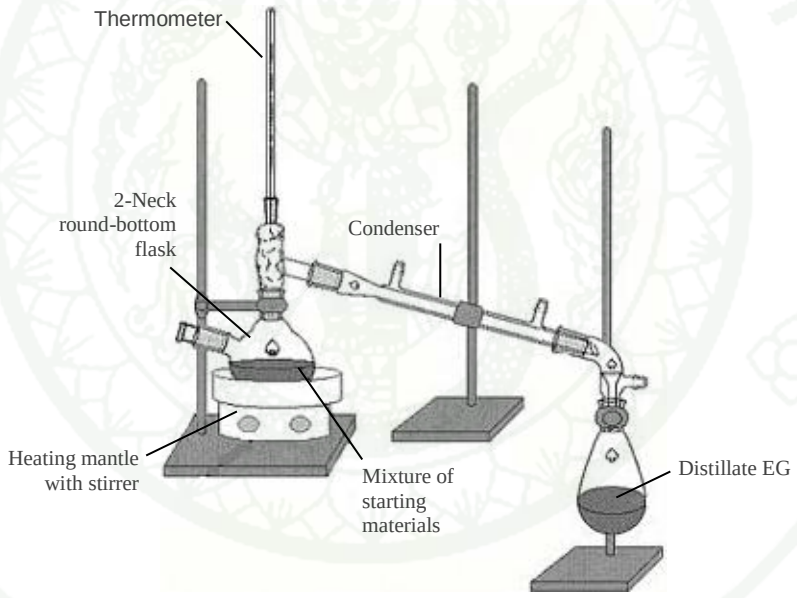

Figure 6 The OOPS equipment setup for the preparation of $MgAl_2O_4$ precursor.

The precursor obtained was then calcined in a furnace (Hope Vally™, LFT 12/75/610) under static air, stepwise, at 500 °C for 5 h, at 750 °C for 5 h, and at 850 °C for 2 h, using 5 °C min^{-1} ramp (Kijjanukij, 2006). The ceramic was manually ground to powder in a mortar. The ceramic powders were kept in a desiccator.

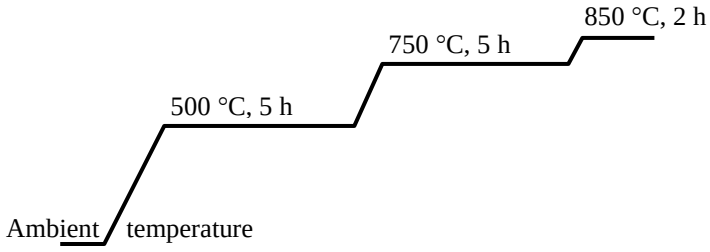

Figure 7 Diagram of the stepwise calcination of $MgAl_2O_4$ precursor.

1.2 Preparation of doped-ceramic $MgAl_2O_4$:Dy(III)

The $MgAl_2O_4$ ceramic was doped with different amounts of Dy(III) from 0.5 to 3.0 %mol. Various amounts of $Dy(C_2H_3O_2)_3$, MgO, Al_2O_3 , and TEA, as listed in Table 1, were placed in a 2-neck, round-bottom flask together with 100 ml of EG solvent. The mixture was heated at 190 °C with continuous stirring for 6 h. During the process, aliquots of 10-ml EG solvent were added from time to time in order to replace the EG lost as distillate. The Dy(III)-doped-$MgAl_2O_4$ precursors were then calcined stepwise as in the Preparation 1.1; that is at 500 °C for 5 h, 750 °C for 5 h, and 850 °C for 2 h, using 5 °C min^{-1} ramp.

1.3 Preparation of doped-ceramic $MgAl_2O_4$:Mn(II)

The Mn(II)-doped $MgAl_2O_4$ ceramic was prepared using the same procedure and conditions as in the preparation of Dy(III)-doped ceramics. The amounts of materials used for preparing 0.50, 0.75, and 1.00% mol Mn(II)-doped $MgAl_2O_4$ ceramics, *i.e.* $Mn(C_2H_3O_2)_2$, MgO, Al_2O_3 , and TEA, are shown in Table 2. The Mn(II)-doped-$MgAl_2O_4$ precursors were calcined stepwise as in the Preparation 1.1.

1.4 Preparation of co-doped-ceramic $MgAl_2O_4$:Dy(III),Mn(II)

A series of co-doped-ceramic $MgAl_2O_4$:Dy(III),Mn(II) was prepared by the same OOPS process and conditions as in the preparation of Dy(III)-doped and Mn(II)-doped ceramics. The amount of Mn(II) dopant in the ceramics varied from 0.10 to

1.00 % mol, whilst that of Dy(III) was kept constant at 1.00 % mol. The amounts of doping and other starting materials: $Dy(C_2H_3O_2)_3$, $Mn(C_2H_3O_2)_2$, MgO, Al_2O_3 , and TEA, are given in Table 3. The Dy(III),Mn(II) co-doped-$MgAl_2O_4$ precursors were calcined stepwise as in the Preparation 1.1.

Table 1 The amounts of $Dy(C_2H_3O_2)_3$, MgO, Al_2O_3, and TEA in the preparation of Dy(III)-doped $MgAl_2O_4$ ceramics.

% Dopant	**$Dy(C_2H_3O_2)_3$**		**MgO**		**Al_2O_3**		**TEA**	
Dy(III)	(mmol)	(g)	(mmol)	(g)	(mmol)	(g)	(mmol)	(ml)
0.50%Dy(III)	0.250	0.0849	49.750	2.0055	50.000	8.0690	150.000	20.00
0.75%Dy(III)	0.375	0.1274	49.625	2.0004	50.000	8.0690	150.000	20.00
1.00%Dy(III)	0.500	0.1698	49.500	1.9954	50.000	8.0690	150.000	20.00
1.50%Dy(III)	0.750	0.2547	49.250	1.9853	50.000	8.0690	150.000	20.00
2.00%Dy(III)	1.000	0.3396	49.000	1.9752	50.000	8.0690	150.000	20.00
2.50%Dy(III)	1.250	0.4246	48.750	1.9652	50.000	8.0690	150.000	20.00
3.00%Dy(III)	1.500	0.5095	48.500	1.9551	50.000	8.0690	150.000	20.00

Table 2 The amounts of $Mn(C_2H_3O_2)_2$, MgO, Al_2O_3, and TEA in the preparation of Mn(II)-doped $MgAl_2O_4$ ceramics.

% Dopant	**$Mn(C_2H_3O_2)_2$**		**MgO**		**Al_2O_3**		**TEA**	
Mn(II)	(mmol)	(g)	(mmol)	(g)	(mmol)	(g)	(mmol)	(ml)
0.50%Mn(II)	0.250	0.0613	49.750	2.0055	50.000	8.0690	150.000	20.00
0.75%Mn(II)	0.375	0.0919	49.625	2.0004	50.000	8.0690	150.000	20.00
1.00%Mn(II)	0.500	0.1225	49.500	1.9954	50.000	8.0690	150.000	20.00

Table 3 The amounts of $Dy(C_2H_3O_2)_3$, $Mn(C_2H_3O_2)_2$, MgO, Al_2O_3 , and TEA for preparing co-doped $MgAl_2O_4$:Dy(III),Mn(II) ceramics.

% Dopant	**$Dy(C_2H_3O_2)_3$**		**$Mn(C_2H_3O_2)_2$**		**MgO**		**Al_2O_3**		**TEA**	
Dy(III), Mn(II)	(mmol)	(g)	(mmol)	(g)	(mmol)	(g)	(mmol)	(g)	(mmol)	(ml)
1.00%Dy(III), 0.10%Mn(II)	0.500	0.1698	0.050	0.0123	49.450	1.9934	50.000	8.0690	150.000	20.00
1.00%Dy(III), 0.50%Mn(II)	0.500	0.1698	0.250	0.0613	49.250	1.9853	50.000	8.0690	150.000	20.00
1.00%Dy(III), 0.75%Mn(II)	0.500	0.1698	0.375	0.0919	49.125	1.9803	50.000	8.0690	150.000	20.00
1.00%Dy(III), 1.00%Mn(II)	0.500	0.1698	0.500	0.1225	49.000	1.9752	50.000	8.0690	150.000	20.00

2. Characterization of undoped and doped $MgAl_2O_4$ ceramics

Before the characterization, the synthesized ceramic powders, both undoped and doped, were dried above 100 °C in an oven for 6 h in order to expel traces of moisture.

2.1 X-ray diffraction spectrometry

The crystal structure of the ceramic powders were characterized by an XRD spectrometer (Jeol™, JDX-3530), using a nickel-filtered CuKα radiation source and operated via software program DIFFRAC.SUITE. The x-ray diffraction patterns were recorded over the 2θ angle of 10-80 degree.

2.2 Scanning electron microscopy

The microscopic structure of the obtained ceramics were examined by a scanning electron microscope (SEM; Phillips™, XL30) operated by software program xT microscope control version 4.1.8.2116, using an acceleration voltage of 20 keV, at a working distance of 15 mm. The powder sample placed on a stub was sputtered-coated with gold to enhance the electrical conductivity. The SEM images (with magnification up to 3k) were taken to distinguish the morphology and the crystalline forms of the ceramics.

2.3 Energy-dispersive X-ray spectrometry

The compositions of the synthesized ceramics were determined and analyzed based on the energy and the intensity of x-ray emitted from the ceramic samples. The x-ray emission spectra of the ceramic powders were recorded by the energy-dispersive x-ray (EDX) detector equipped to the Phillips™-XL30 SEM. The data analysis was acquired from a software program The Microanalysis Suite (INCA Suite version 4.15).

3. Photoluminescence study of undoped and doped $MgAl_2O_4$ ceramics

The photoluminescent properties of the prepared ceramics were investigated using a spectrofluorometer (PerkinElmer™, LS55). The emission spectra were recorded over the range of 350-800 nm at a fixed excitation wavelength of 350 nm and 302 nm for Dy(III) and Mn(II) dopant, respectively. The characteristic spectra were observed and the wavelength that yielded the maximum fluorescence intensity, λ_{em}, was located.

RESULTS AND DISCUSSION

1. Preparation of $MgAl_2O_4$ ceramics: undoped, and doped with Dy(III) and Mn(II)

The precursor obtained was a clear brown-colored, hard and rigid polymer-like material.

Figure 8 The polymer-like $MgAl_2O_4$ precursor before the calcination.

The ceramic materials were obtained after stepwise calcinations under static air. The solid lump was then manually ground in an alumina mortar to produce ceramic powder. The un-doped and Dy(III)-doped $MgAl_2O_4$ ceramics are of white color, whilst those of Mn(II)-doped ceramics vary from pale pink, beige, to brown.

Figure 9 Dy(III)-doped $MgAl_2O_4$ ceramic powders.

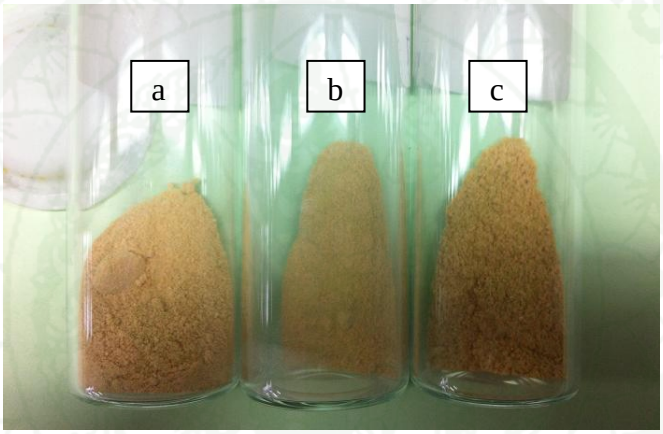

Figure 10 Mn(II)-doped $MgAl_2O_4$ ceramic powders: a) 0.50%; b) 0.75%; c) 1.00%.

Figure 11 Dy(III),Mn(II)-codoped $MgAl_2O_4$ ceramic powders:

a) 1.00%Dy(III), 0.10%Mn(II); b) 1.00%Dy(III), 0.50%Mn(II)

c) 1.00%Dy(III), 0.75%Mn(II); d) 1.00%Dy(III), 1.00%Mn(II)

2. Characterization of undoped and doped $MgAl_2O_4$ ceramics

2.1 X-ray diffraction patterns

2.1.1 X-ray diffraction pattern of undoped $MgAl_2O_4$

The XRD pattern of the prepared $MgAl_2O_4$ ceramic is displayed in Figure 12 together with the patterns of $MgAl_2O_4$ and γ-Al_2O_3 acquired from the JCPDS files with which the Jeol™ XRD spectrometer is installed. Three strong peaks are found at 2θ angles of 37.01, 45.01, and 65.54 degree, all of which also appear in the patterns of both JCPDS files: the No. 21-1152 of $MgAl_2O_4$ spinel, and the No. 29-63 of γ-Al_2O_3 . The XRD patterns of the prepared $MgAl_2O_4$ and of the γ-Al_2O_3 are, however, considerably different. The pattern is found similar to that of the JCPDS file No. 21-1152 — that is all the peaks appear at the same 2θ positions — indicating the presence of the cubic structure of $MgAl_2O_4$ spinel.

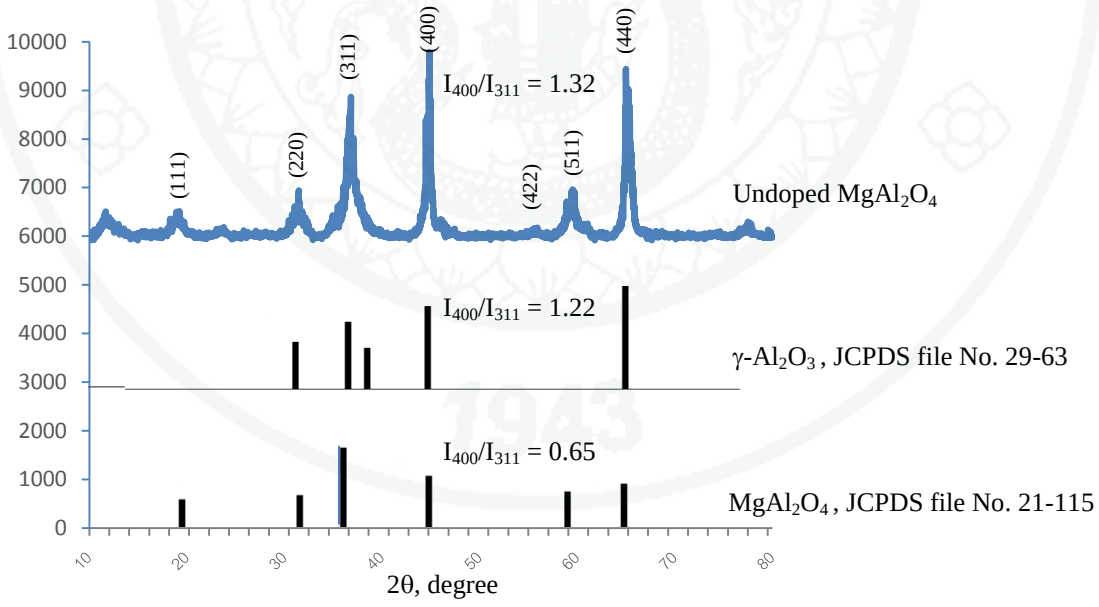

Figure 12 The XRD pattern of the undoped $MgAl_2O_4$ ceramic powder.

Nevertheless the intensity ratio of the peaks at 2θ = 37.01 and 45.01 degree (which corresponding to the diffraction at lattice planes 311 hkl and 400 hkl,

respectively) is noticeably altered. The intensity ratio I_{400}/I_{311} of the prepared ceramic is 1.32 (1:0.76) which is two times higher than that of 0.65 (1:1.53) found in the pattern of a pure $MgAl_2O_4$ spinel (JCPDS No. 21-1152). A high I_{400}/I_{311} ratio of 1.22 (1:0.82) is observed in the XRD pattern of γ-Al_2O_3 . This suggested that the synthesized ceramic was not entirely of $MgAl_2O_4$, but γ-Al_2O_3 was also present. The existence of this γ-Al_2O_3-$MgAl_2O_4$ solid solution was possibly due to the low-temperature calcination (Waldner *et al.*, 1996). It was previously reported that pure $MgAl_2O_4$ spinel ceramics were attained after calcining the $MgAl_2O_4$ precursor derived from OOPS at 1,300 °C for 2h (Laobuthee *et al.*, 2000). This study had attempted a stepwise calcination (Kijjanukij, 2006) at lower temperatures (500-850° C) with prolonging time of 12 h in order to avoid the product ceramics being fused at high temperatures. The attempt resulted in the incomplete transformation of the OOPS-prepared precursor to $MgAl_2O_4$ spinel. Consequently, the synthesized ceramic was composed of $MgAl_2O_4$ spinel and γ-Al_2O_3 as it was evident in the XRD pattern. Hence, complete $MgAl_2O_4$ ceramic was unattainable via stepwise calcination under the chosen working conditions.

2.1.2 X-ray diffraction patterns of doped $MgAl_2O_4$ ceramics

The XRD patterns of the singly-doped ceramics, *i.e.* $MgAl_2O_4$:Dy(III) and $MgAl_2O_4$:Mn(II), and the co-doped $MgAl_2O_4$:Dy(III),Mn(II) were obtained under the instrumental conditions used for the undoped $MgAl_2O_4$. The XRD patterns of $MgAl_2O_4$:Dy(III), $MgAl_2O_4$:Mn(II), and of $MgAl_2O_4$:Dy(III),Mn(II) are presented in Figures 13, 14, and 15, respectively. All patterns resemble that of JCPDS $MgAl_2O_4$ in the diffraction angles — the 2θ positions, implying the cubic structure of $MgAl_2O_4$ spinel. The peak intensity ratio, I_{400}/I_{311} , of the doped ceramics was found to decrease with the increasing concentration of the dopant. The I_{400}/I_{311} ratio had dropped from 1.32 of the undoped $MgAl_2O_4$ to 0.92 of the 3%-Dy(III)-doped $MgAl_2O_4$ (Figure 13), to 0.89 of the 1%-Mn(II)-doped $MgAl_2O_4$ (Figure 14), and to an average 0.93 of the co-doped Dy(III),Mn(II) (Figure 15). The I_{400}/I_{311} ratio of the doped ceramics is, however, still higher than that 0.65 of a pure $MgAl_2O_4$ spinel. The produced ceramics were thus composed of doped $MgAl_2O_4$ spinel and γ-Al_2O_3 as it was in the case of undoped $MgAl_2O_4$. The lowered I_{400}/I_{311} ratios suggested a higher proportion of spinel in the

doped ceramics than that in the undoped one. The decrease in I_{400}/I_{311} ratio might concern the involvement of the dopants in the transformation of the precursors to $MgAl_2O_4$ spinel during the stepwise calcination. The matter may be further explored.

The characteristic sharp peaks in the XRD pattern of the undoped $MgAl_2O_4$ also changed upon doping. The peaks are visibly broadened with reduced height. This can be contributed to the distortion of the spinel crystal structure occurred when a dopant ion replaces the Mg^{2+} ion. The slightly broader peaks are found from Dy(III) doping (Figure 13), compared to those of Mn(II) doping (Figure 14). The larger size of Dy^{3+} (105.2 pm) replacing Mg^{2+} (86 pm) is likely to cause more distortion than does the smaller Mn^{2+} (78.5 pm).

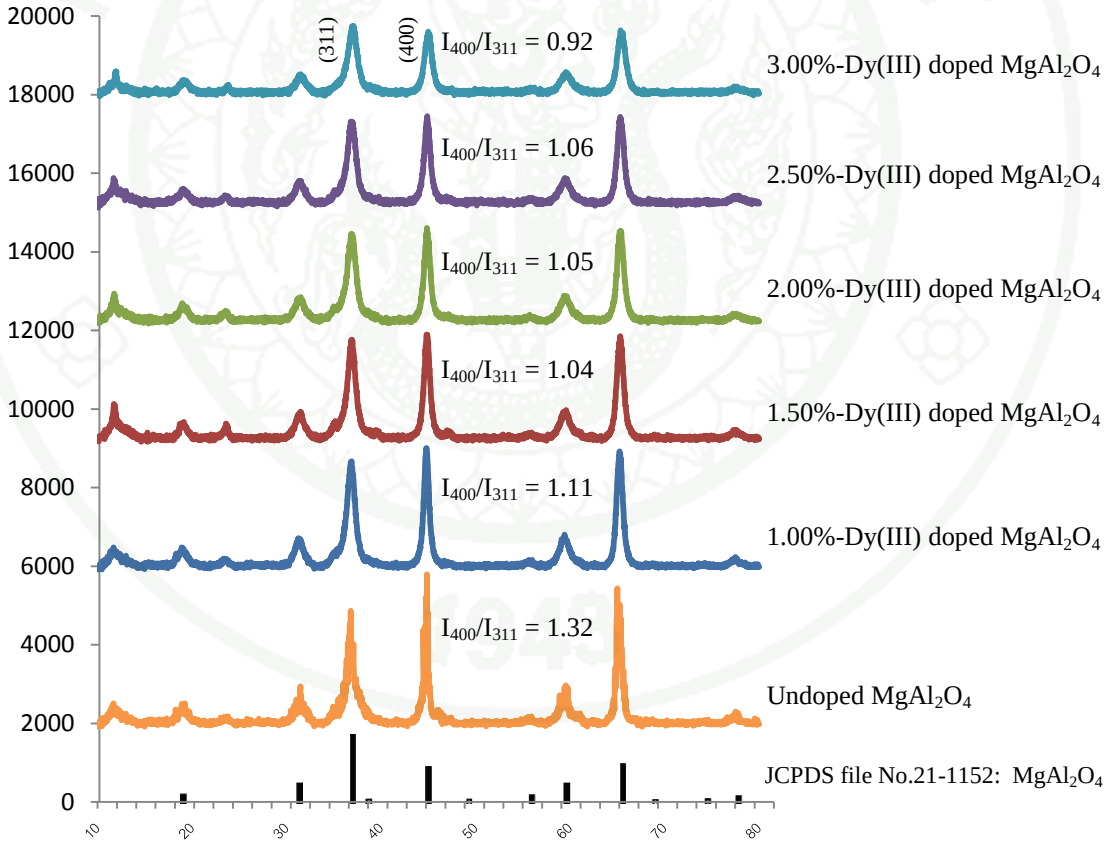

Figure 13 The XRD patterns of the Dy(III)-doped $MgAl_2O_4$ ceramic powders.

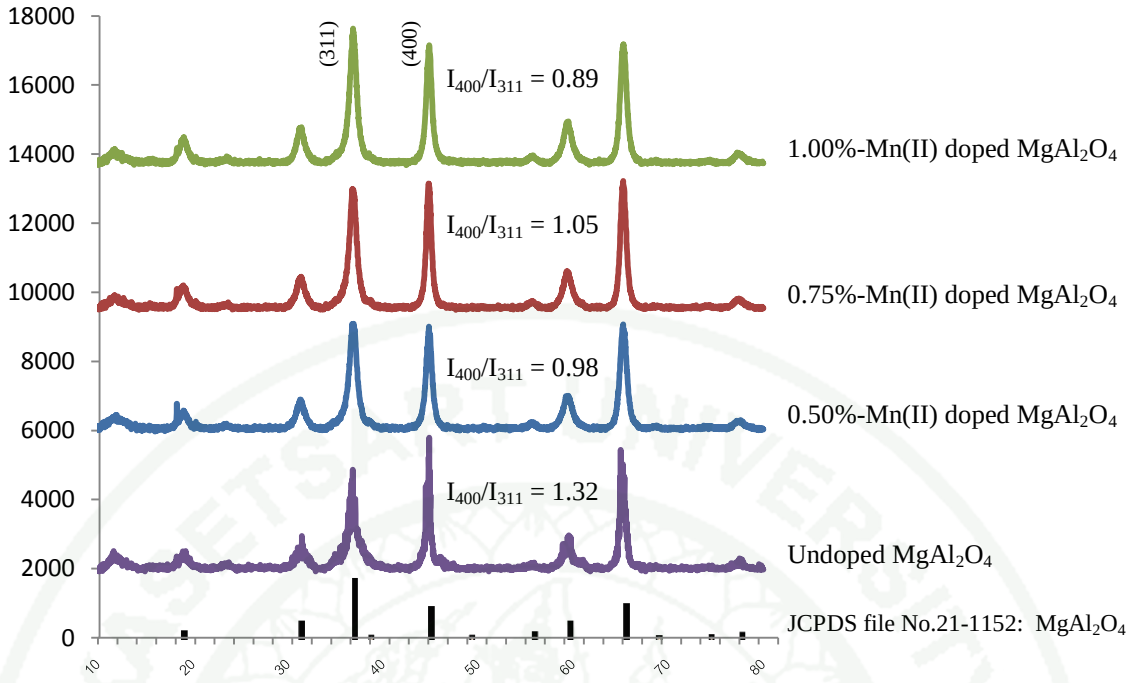

Figure 14 The XRD patterns of the Mn(II)-doped $MgAl_2O_4$ ceramic powders.

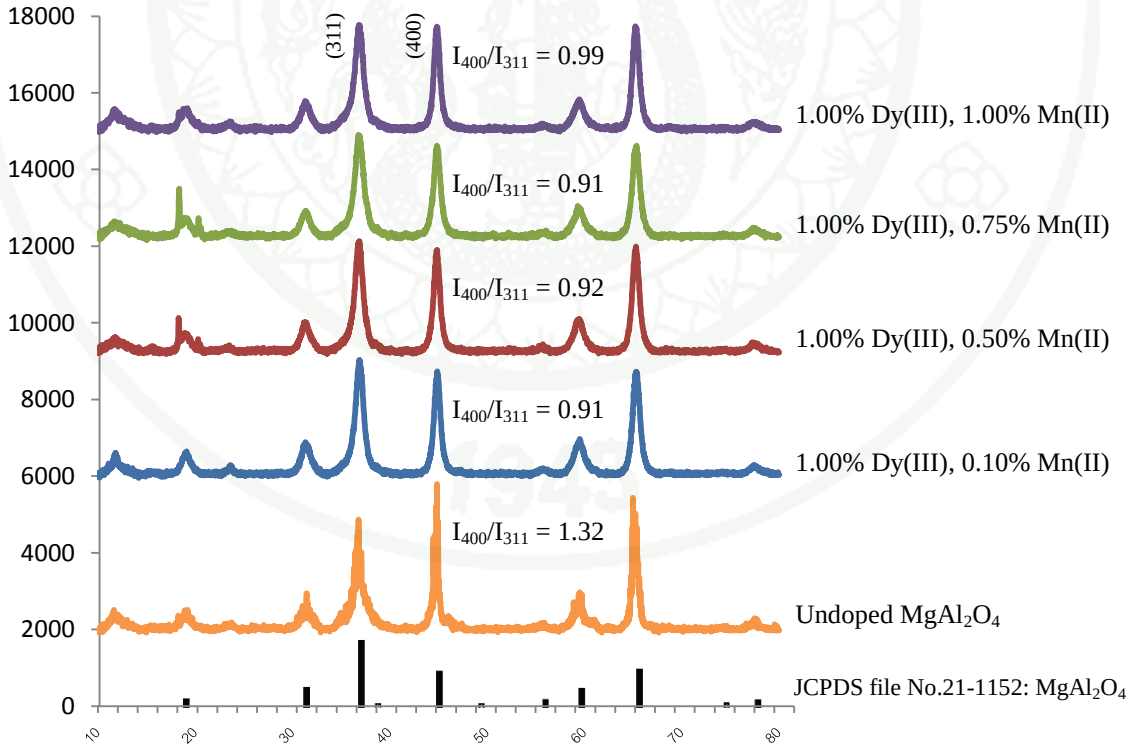

Figure 15 The XRD patterns of Dy(III),Mn(III)-codoped $MgAl_2O_4$ ceramic powders.

2.2 Scanning electron microscopic images

The morphology and the crystalline forms of the prepared ceramics can be viewed from the 3k-magnification SEM images. The image of undoped $MgAl_2O_4$ in Figure 16-a shows the blocky particles in irregular shapes, possibly a result of the agglomeration occurring in the calcination process of the precursor. The crystalline form of hexagonal shape can also be spotted (see the inset). The hexagonal crystalline form is superbly revealed in Figure 16-b — the image of 1%-Dy(III)-doped $MgAl_2O_4$. Figure 16-c exhibits the microstructure of the Mn(II)-doped spinel powders, showing the blocky particles with uneven shapes which resembles the undoped $MgAl_2O_4$. The Dy(III)-Mn(II) co-doped ceramics have quite a distinctive morphology as displays in Figure 16-d; fiber-like shape, several μm in length, co-exist with the blocky particles.

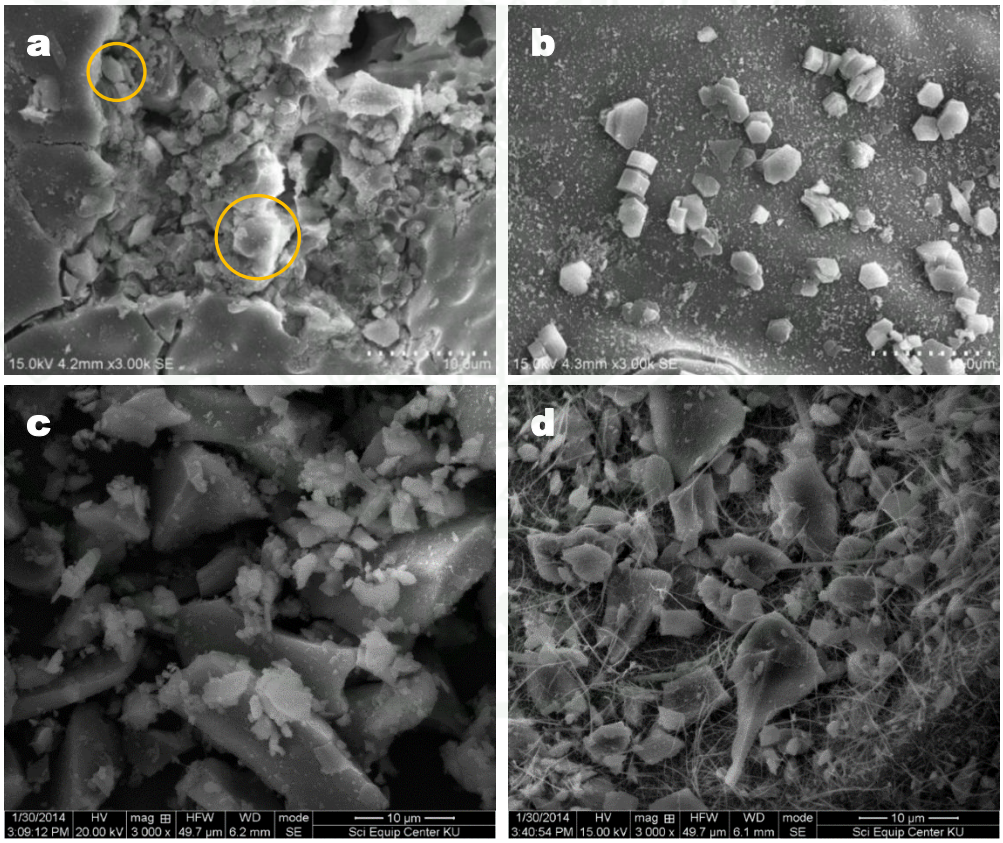

Figure 16 The SEM images: a) undoped $MgAl_2O_4$; b) 1%-Dy(III)-doped $MgAl_2O_4$; c) 0.50%-Mn(II)-doped $MgAl_2O_4$; d) 1.00%Dy(III),0.50%Mn(II)-codoped $MgAl_2O_4$.

2.3 Energy dispersive x-ray emission spectrometry

The composition of the produced ceramics was analyzed and determined by EDX method. The EDX spectral analysis was acquired from the software INCA Suite version 4.15 for microanalysis — designed for Oxford Instruments. The EDX spectra are presented, with the weight and atomic percentages of the constituents, in Figures 17-19. The x-ray lines of the ceramic samples conform to the components of the synthesized ceramics, namely Mg, Al, O, and the dopants Dy and Mn. Being the major components, intense x-rays were found in the emission lines of Mg, Al, and O; whereas the x-rays emitted by the dopants Dy and Mn were of low intensity. The percentage of the components was agreeable with the stoichiometric compositions of the ceramics. The atomic percentages of the dopant(s) in all doped ceramics were found to be in accordance with the mole percentage of that dopant added at the start of preparation. The % doping is 99.26 ± 25.91 at 95% confidence limit, implying an effective doping procedure. The amounts of dopants added and found are summarized in Table 4.

Table 4 Percentages of dopants added and found in the doped and codoped ceramics.

Mol% Added		**Atomic% Found**		**Normalized Atomic%**		**Doping**	**Error**
Dy(III)	Mn(II)	Dy(III)	Mn(II)	Dy(III)	Mn(II)	%	%
1.50	–	0.24	–	1.20	–	80.0	–20.0
2.00	–	0.43	–	2.15	–	107.5	+7.5
2.50	–	0.49	–	2.45	–	98.0	–2.0
3.00	–	0.63	–	3.15	–	105.0	+5.0
–	0.50	–	0.11	–	0.55	110.0	+10.0
–	0.75	–	0.12	–	0.60	80.0	–20.0
–	1.00	–	0.17	–	0.85	85.0	–15.0
1.00	0.10	0.17	0.01	1.00	0.06	58.8*	–41.2
1.00	0.50	0.18	0.09	1.00	0.50	100.0	–
1.00	0.75	0.13	0.11	1.00	0.85	112.8	+12.8
1.00	1.00	0.14	0.16	1.00	1.14	114.3	+14.3

*Outlier.

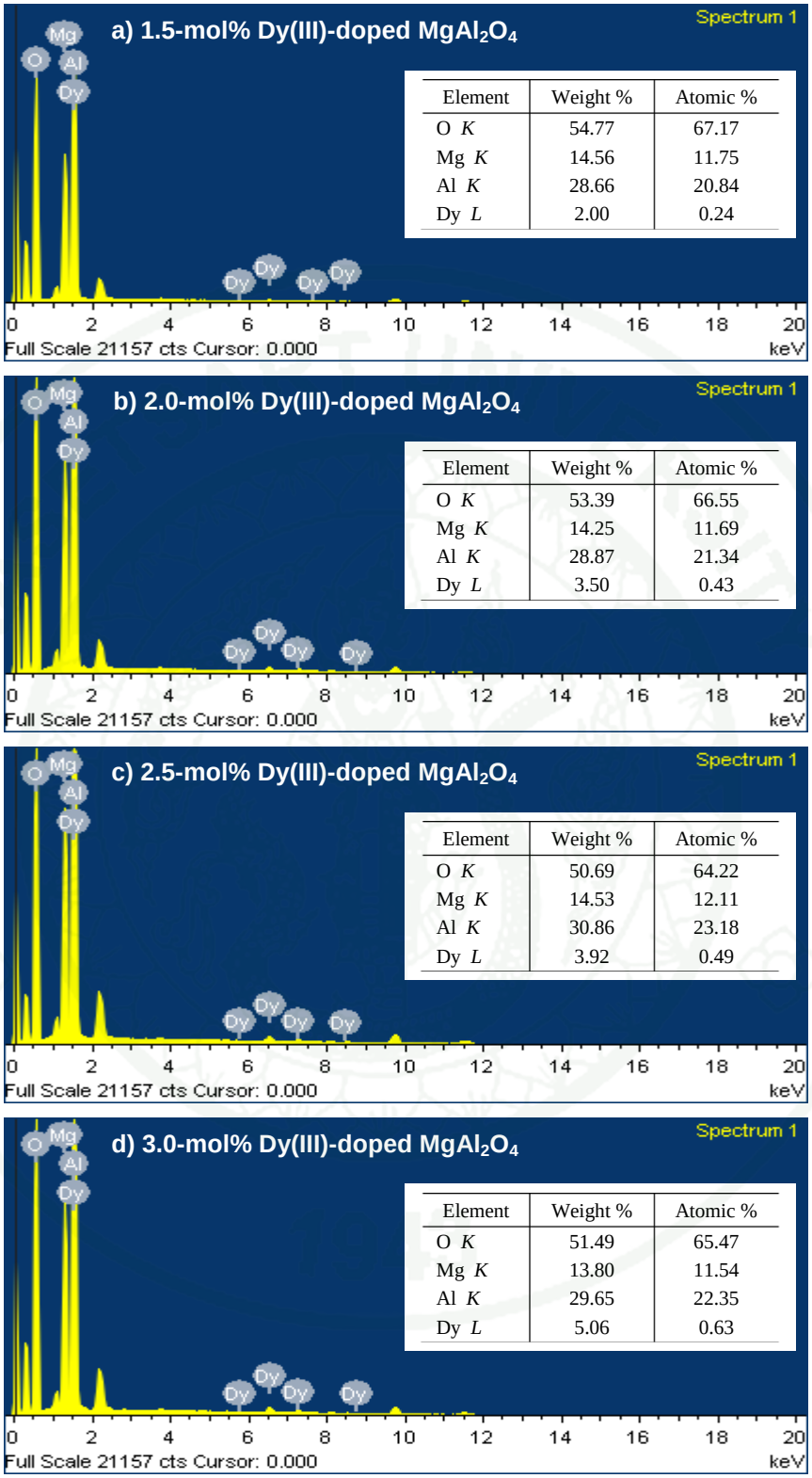

Figure 17 The EDX spectra and analysis of mol%Dy(III)-doped $MgAl_2O_4$ ceramics: a) 1.5 mol% , b) 2.0 mol% , c) 2.5 mol% , and d) 3.0 mol% .

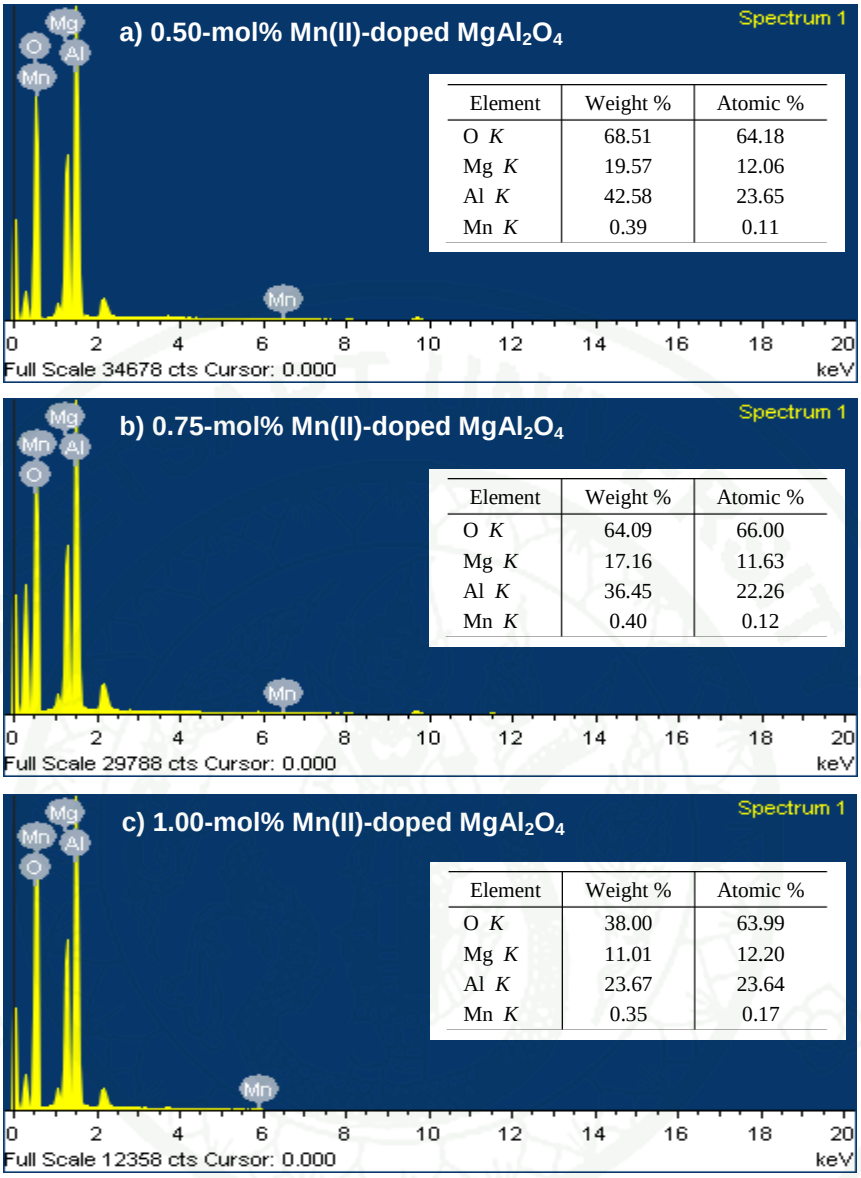

Figure 18 The EDX spectra and analysis of mol%Mn(II)-doped $MgAl_2O_4$ ceramics: a) 0.50 mol% , b) 0.75 mol% , and c) 1.00 mol% .

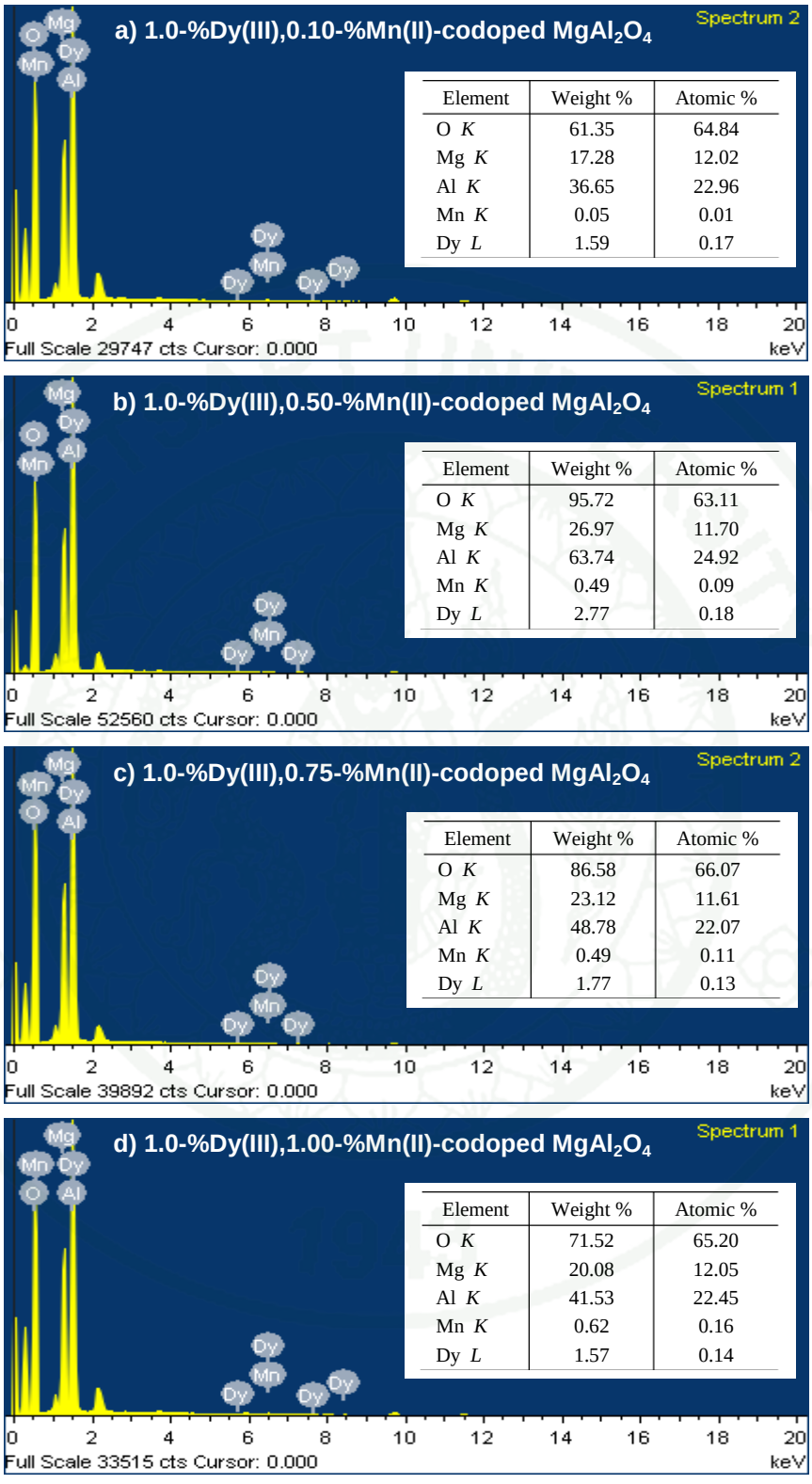

Figure 19 The EDX spectra and analysis of 1.0-%Dy(III),Mn(II)-codoped $MgAl_2O_4$: a) 0.10 %Mn(II), b) 0.50 %Mn(II), c) 0.75 %Mn(II), and d) 1.00 %Mn(II).

3. Photoluminescence study of undoped and doped $MgAl_2O_4$ ceramics

3.1 Photoluminescence of Dy(III)-doped $MgAl_2O_4$ ceramics

3.1.1 Emission of $MgAl_2O_4$:Dy(III) ceramics

The emission spectra of the Dy(III)-doped ceramics in Figure 20 were recorded by a spectrofluorometer, PerkinElmer™ LS55 controlled by FL WinLab solfware, over the wavelength range of 450-700 nm using a pre-scanned excitation wavelength of 350 nm. The Dy(III)-doped $MgAl_2O_4$ ceramics exhibits a yellow fluorescence at λ_{em} of 574.5 nm which is corresponding to the $^4F_{9/2} \rightarrow {}^6H_{13/2}$ transition of Dy(III); whilst the undoped $MgAl_2O_4$ does not offer fluorescence. The yellow fluorescence of Dy(III) found in this work concurs with those previously reported (Karabulut *et al*., 2014; Omkaram *et al*., 2009; Lai *et al*., 2008; Maia *et al*., 2008). The photoluminescence of Dy(III) phosphor can be described as shown in the schematic diagram of Figure 21. Upon absorbing a quantize photon energy, $h\upsilon$, Dy(III) in the Dy(III)-doped $MgAl_2O_4$ is promoted from the electronic ground state $^6H_{15/2}$ to the higher energy excited states. The excited electrons of Dy(III) then relax to the electronic excited state $^4F_{9/2}$ via non-radiative process, which instantly follows by a radiative transition from the excited state $^4F_{9/2}$ to the $^6H_{13/2}$ ground state emitting a yellow fluorescence at the wavelength of 574.5 nm. The λ_{em} of 574.5 nm was used subsequently for the fluorescence measurement of Dy(III)-doped ceramics in this work.

According to the forced electric-dipole principle, the $^4F_{9/2} \rightarrow {}^6H_{13/2}$ transition occurred only in the low symmetrical surroundings with no inversion centre (Wu *et al.*,2006). This suggests that under the doping conditions, Dy(III) ion has entered the host lattice $MgAl_2O_4$ by replacing Mg(II) in the tetrahedral sites. From the aspect of ionic radius, the replacement of 105.2-pm Dy(III) to the 86.0-pm Mg(II) is preferable, compared to that of Dy(III) to the 67.5-pm Al(III).

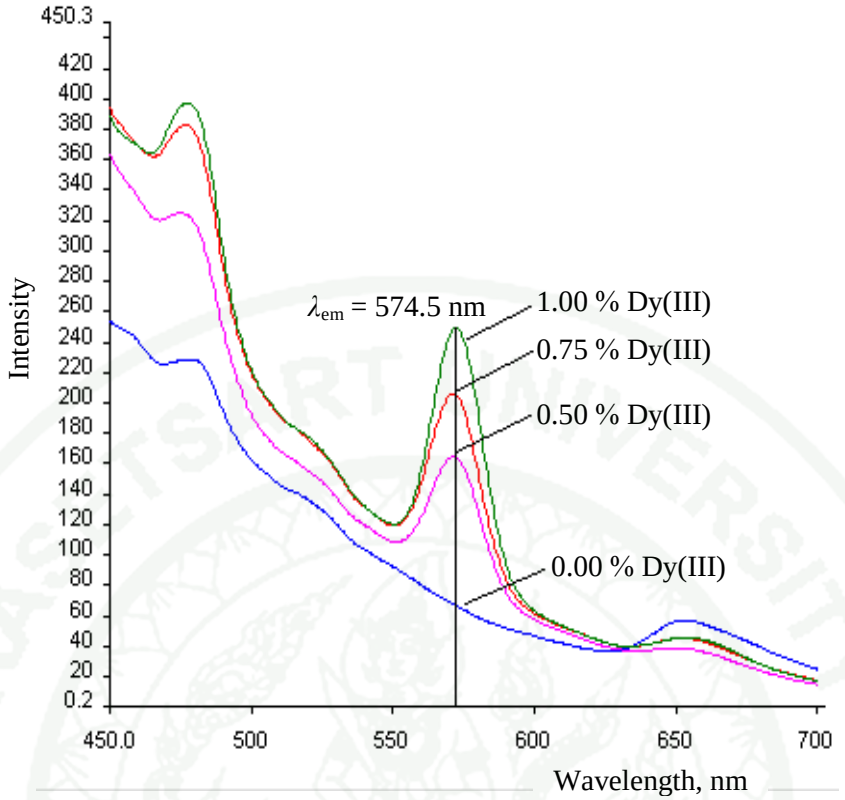

Figure 20 Emission spectra of $MgAl_2O_4$ doped with various amounts of Dy(III).

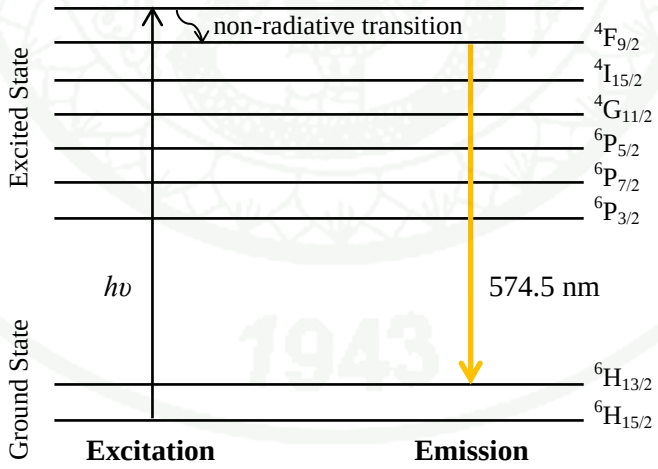

Figure 21 Photoluminescence of Dy(III) phosphor in $MgAl_2O_4$:Dy(III) ceramics.

The influence of Dy(III) on the fluorescence of Dy(III)-doped $MgAl_2O_4$ ceramics was examined by varying the amount of Dy(III) in the ceramics from 0.5 to 3.0 mol% Dy(III). The fluorescence spectra were then recorded (Appendix Figure A1). Although the emission spectral characteristic remains the same, but the fluorescence intensity at λ_{em} 574.5 nm changes with the Dy(III) concentration as the plot shown in Figure 22. The fluorescence was found to increase with the increasing concentration up to 2.0 mol% of Dy(III). The decrease thereafter can be attributed to the concentration quenching phenomenon which is mainly caused by resonant cross-relaxation — the energy is transferred from one photon-emitting Dy(III) to another neighboring Dy(III), thus quenches the fluorescence. With the concentration continued to increase, Dy(III) increasingly quenched its own fluorescence. This self-quenching resulted in the decrease of the fluorescence intensity. The amount of dopant, both Dy(III) and Mn(II), used in the subsequent doping was retained at ≤1.0 mol% as to avoid the concentration quenching.

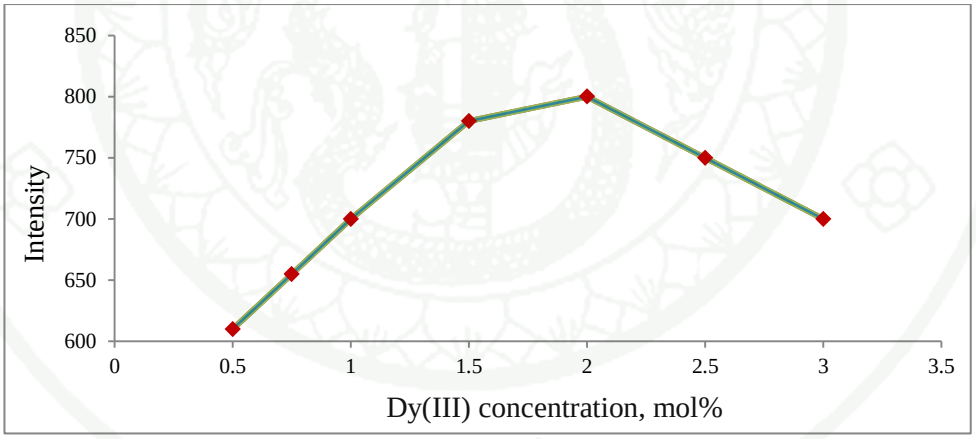

Figure 22 Effect of Dy(III) concentration on the fluorescence of $MgAl_2O_4$:Dy(III).

3.1.2 Excitation of $MgAl_2O_4$:Dy(III) ceramics

The excitation spectrum, measured at the λ_{em} 574.5 nm, of 1%-Dy(III)-doped $MgAl_2O_4$, displays the excitation bands of 4f–4f transitions of Dy(III) over the range of 320-500 nm. Six excitation peaks, *i.e.* 320, 350, 380, 420, 450, and 480 nm in Figure 23, can be identified and assigned to the transitions from the ground energy level of $^6H_{15/2}$ to the higher energy levels $^6P_{3/2}$, $^6P_{7/2}$, $^6P_{5/2}$, $^4G_{11/2}$, $^4I_{15/2}$, and $^4F_{9/2}$ of Dy(III), respectively (Omkaram *et al*., 2009). The wavelength of 350.8 nm was used as the excitation wavelength, λ_{ex} , for Dy(III)-doped ceramics in the subsequent works as providing the highest fluorescence intensity.

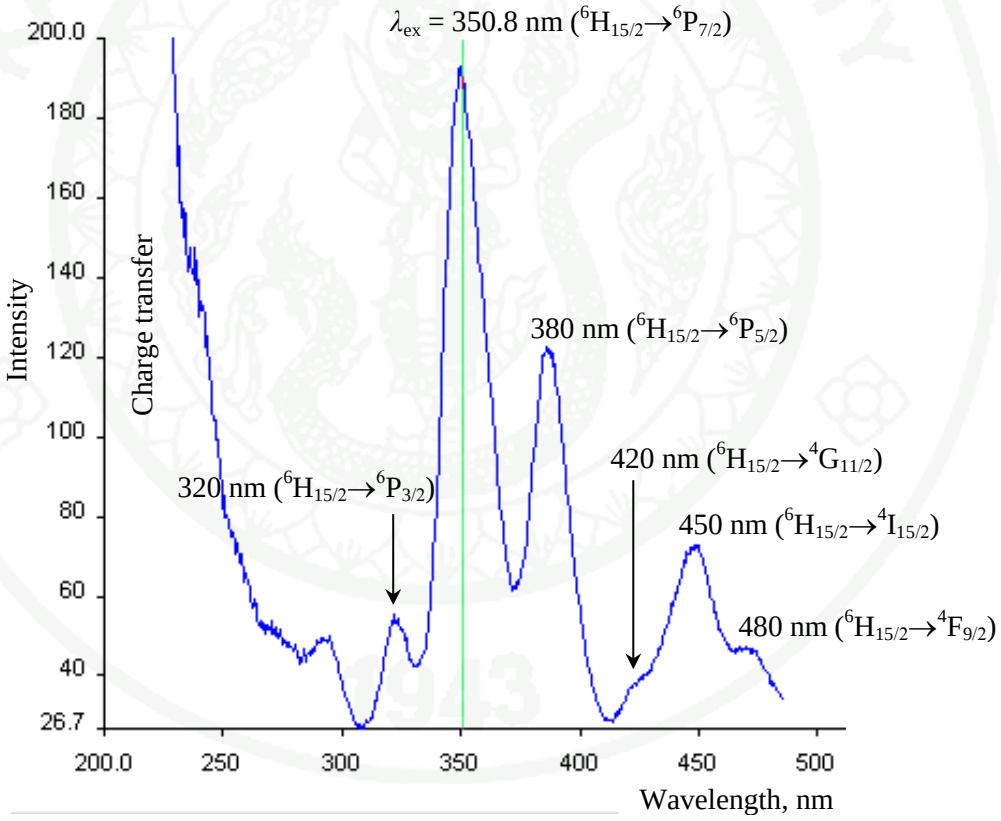

Figure 23 Excitation spectrum of $MgAl_2O_4$ doped with 1% Dy(III) phosphor.

3.2 Photoluminescence of Mn(II)-doped $MgAl_2O_4$ ceramics

3.2.1 Emission of $MgAl_2O_4$:Mn(II) ceramics

The emission spectra of the $MgAl_2O_4$:Mn(II) ceramics in Figure 23, recorded by a PerkinElmer™ LS55 spectrofluorometer using a pre-scanned λ_{ex} of 302 nm, display strong emission peaks at the wavelength 658 nm whereas the undoped $MgAl_2O_4$ ceramic gives no fluorescence. The reddish-orange fluorescence is resulted from the $^4T_1 \rightarrow {}^6A_1$ internal transition of Mn(II), as the diagram shown in Figure 24. Upon absorbing a quantize photon energy, $h\upsilon$, Mn(II) in the Mn(II)-doped $MgAl_2O_4$ is stimulated from the electronic ground state $^6A_1$ to the higher energy excited states. The excited electrons of Mn(II) then relax via a series of non-radiative process to the lowest energy level $^4T_1$ of the excited state. A radiative transition from $^4T_1$ to the ground state $^6A_1$ follows immediately, emitting a reddish-orange fluorescence at the wavelength of 658 nm. The λ_{em} of 658 nm was used subsequently for the fluorescence measurement of Mn(II)-doped ceramics in this work.

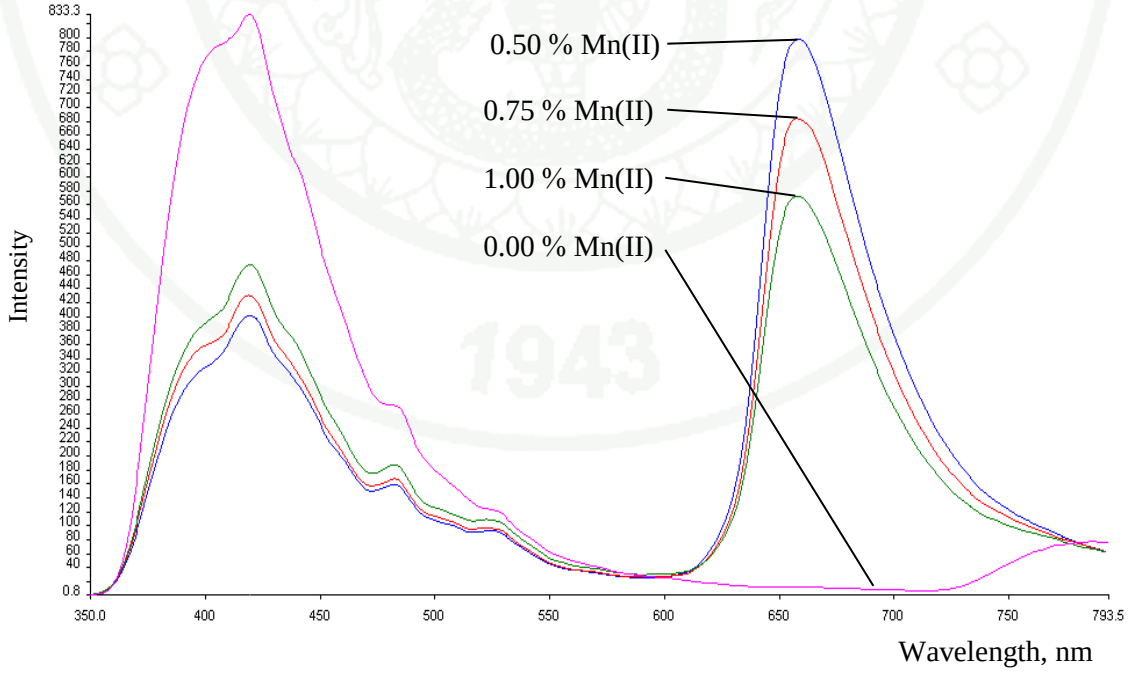

Figure 24 Emission spectra of $MgAl_2O_4$ doped with various amounts of Mn(II).

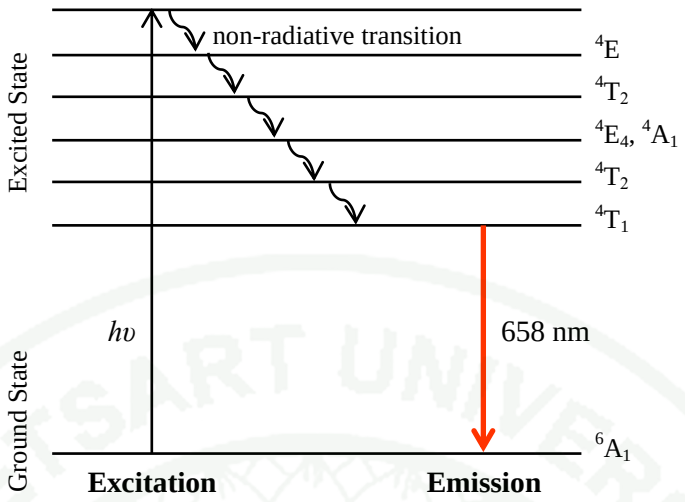

Figure 25 Photoluminescence of Mn(II) phosphor in $MgAl_2O_4$:Mn(II) ceramics.

The $^4T_1 \rightarrow {}^6A_1$ transition usually gives out emission between 500 to 700 nm, ranging from green to red fluorescence. The coordination number and the ligand field strength of Mn^{2+} ion in different matrix systems are associated to the distinct splitting of the $3d^5$energy levels of Mn^{2+} (Tanabe and Sugano, 1954). For examples, green fluorescence is obtained from Zn_2SiO_4:Mn(II) in which Mn^{2+} has the coordination number of four (tetrahedral coordination) with a weak ligand field (Sohn *et al*., 1999), so as the emission of Zn_2GeO_4:Mn(II) found at λ 524 nm (Palumbo *et al*., 1970). On the contrary, having octahedral coordination (coordination number of 6) with a strong crystal field, Mn^{2+} in $Ca_5(PO_4)_3F$:Mn(II) emits orange fluorescence (Shinoya *et al*., 1999); while the red luminescence of $Sr_3MgSi_2O_8$:Mn(II) is found at 690 nm (Yao *et al*., 1997), and that of ZnSe:Mn(II) is yellowish orange at 585 nm (Norris *et al*., 2001). Emitting reddish-orange fluorescence at 658 nm, Mn^{2+} in the prepared $MgAl_2O_4$:Mn(II) ceramics of the current work is of octahedral coordination. It can be deduced that Mn(II) ions enter the $MgAl_2O_4$ host by replacing Al(III) ions in the octahedral site (Kawano *et al*., 2009).

3.2.2 Excitation of $MgAl_2O_4$:Mn(II) ceramics

The excitation spectrum of $MgAl_2O_4$ doped with 1% Mn(II), recorded in Figure 25, was monitored at the emission wavelength (λ_{em}) of 658 nm which had obtained from the former experiment. The spectrum displays broad-banded characteristic peaks assigned to the excitation of Mn^{2+} ion from the electronic ground state $^6A_1$ to the higher excited state. It was found that the excitation spectrum precisely coincided with the absorption spectrum reported before by Tomita and coworkers (2004). Four excitation peaks at the wavelengths of 302, 385, 425, and 450 were identified and assigned to the internal transitions of Mn^{2+} from the ground energy level $^6A_1$ to the higher levels of $^4T_1/^4E$, $^4T_2$, $^4A_1/^4E$, and $^4T_2$, respectively. The wavelength of 302 nm, at which the highest fluorescence intensity was achieved, was selected as the excitation wavelength, λ_{ex} , for Mn(II)-doped ceramics in the following works.

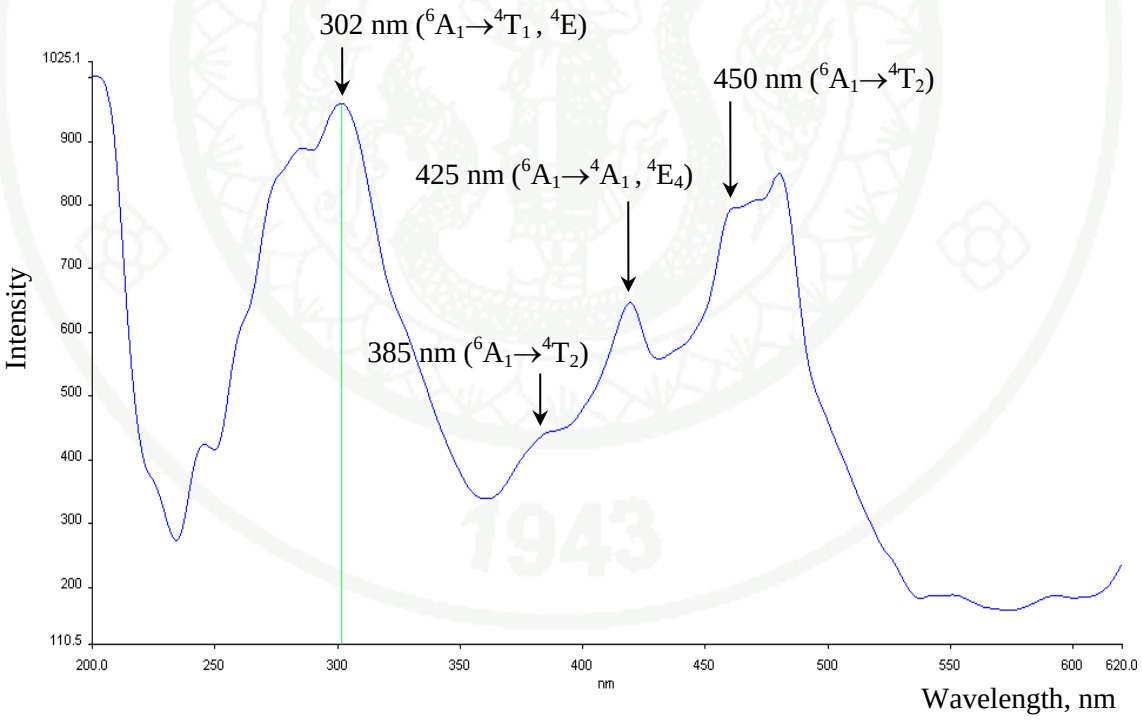

Figure 26 Excitation spectrum of $MgAl_2O_4$ doped with 1% Mn(II) phosphor.

3.3 Photoluminescence of codoped $MgAl_2O_4$:Dy(III),Mn(II) ceramics

The photoluminescence spectra of $MgAl_2O_4$ codoped with a fixed 1% Dy(III) and Mn(II), of which the concentration is varied, using a λ_{ex} of 350.8 nm are shown in Figure 27. The spectra display the combining characteristics of Dy(III) and Mn(II) phosphors, as seen in Figures 20 and 23, respectively. Two strong emission bands are observed. The band at 574.5 nm is identified with the $^4F_{9/2} \rightarrow {}^6H_{13/2}$ transition of Dy(III), whilst the other one at 658 nm is corresponded to the $^4T_1 \rightarrow {}^6A_1$ transition of Mn(II). It was found that the fluorescence intensity of Dy(III) at $\lambda_{em,Dy(III)}$ 574.5 nm dropped drastically in the presence of Mn(II). The decrease is visibly detected from the spectra in Figure 26: a) without Mn(II) doping; b) with 0.10%-Mn(II) doping; and c) 0.50%-Mn(II) doping. It appeared that the fluorescence of Dy(III) was entirely quenched with the doping of Mn(II) from 0.50% up, as seen in the spectra c), d) 0.75% Mn(II); and e) 1.00% Mn(II). On the contrary, the fluorescence of Mn(II) at $\lambda_{em,Mn(II)}$ 658 nm increases appreciably in the presence of Dy(III) as shown in Figure 27. The energy transfer between Mn(II) and Dy(III) may have accounted for the effect.

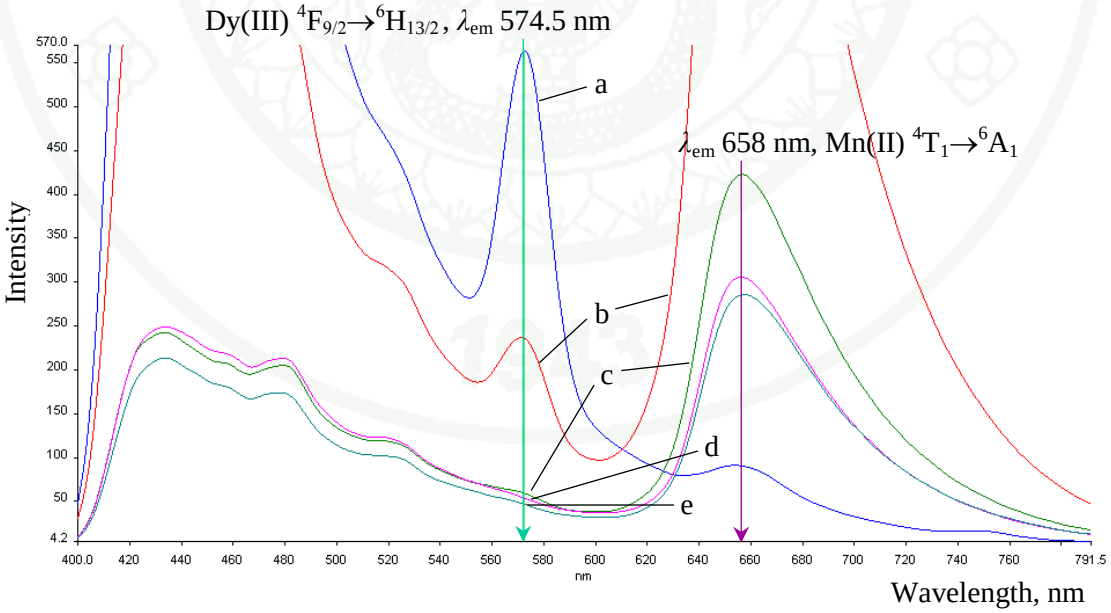

Figure 27 Emission spectra of $MgAl_2O_4$ codoped with 1.0% Dy(III) and Mn(II): a) 0.00% Mn(II); b) 0.10% Mn(II); c) 0.50% Mn(II); d) 0.75% Mn(II); and e) 1.00% Mn(II).

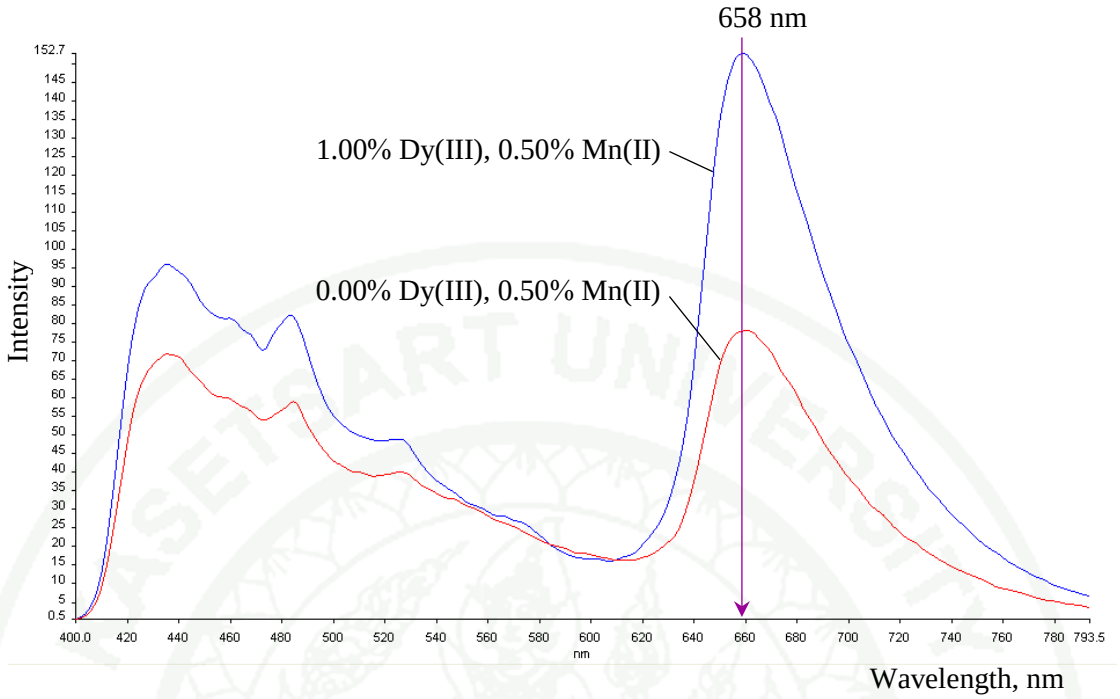

Figure 28 Emission spectra of 0.50%-Mn(II)-doped $MgAl_2O_4$ codoped with 1% Dy(III), and without Dy(III) codoping.

The decrease in fluorescence intensity of Dy(III) along with the increasing fluorescence of Mn(II) suggests an energy transfer from the photon-emitting Dy(III) to Mn(II). The Dy(III)→Mn(II) energy transfer process can be described by a schematic diagram in Figure 28. The excited Dy(III) ions normally relax via a non-radiative process to the $^4F_{9/2}$ energy level, from where the still-excited Dy(III) returns to $^6H_{13/2}$ ground level instantly by radiative transition, giving out yellow fluorescence of 574.5 nm (as depicted in Figure 21). The presence of Mn(II), however, quenches the Dy(III) fluorescence. At low concentrations of Mn(II), part of the energy of the excited Dy(III) at $^4F_{9/2}$ level is directly transferred to Mn(II) ions in the ^4E level. The excited Mn(II) ions then relax to the lowest excited energy level $^4T_1$ through a series of non-radiative process prior to a radiative relaxation from $^4T_1$ to the ground state $^6A_1$. Therefore, the fluorescence of Mn(II) phosphor is enhanced by Dy(III); or *vice versa*, the fluorescence of Dy(III) is diminished by Mn(II). As the %doping of Mn(II) increased, the energy of the excited Dy(III) was entirely transferred to the Mn(II), thus completely quenched the fluorescence at 574.5 nm. In the fluorescence enhancing aspect, Dy(III) plays a role of

sensitizer to the activator part of Mn(II) in the codoped $MgAl_2O_4$:Dy(III),Mn(II) ceramics. The similar effect of codoping Dy(III),Mn(II) on the photoluminescence behavior of $SrAl_2O_4$ ceramics has been reported recently (Karabulut *et al*., 2014). In addition, the chosen λ_{ex} of 350.8 nm in the current study had further assisted the fluorescence enhancement of the codoped $MgAl_2O_4$:Dy(III),Mn(II) ceramics, since the λ_{ex} 350.8 nm is equivalent to the quantize energy for directly exciting Mn^{2+} ions to the ^4E energy level.

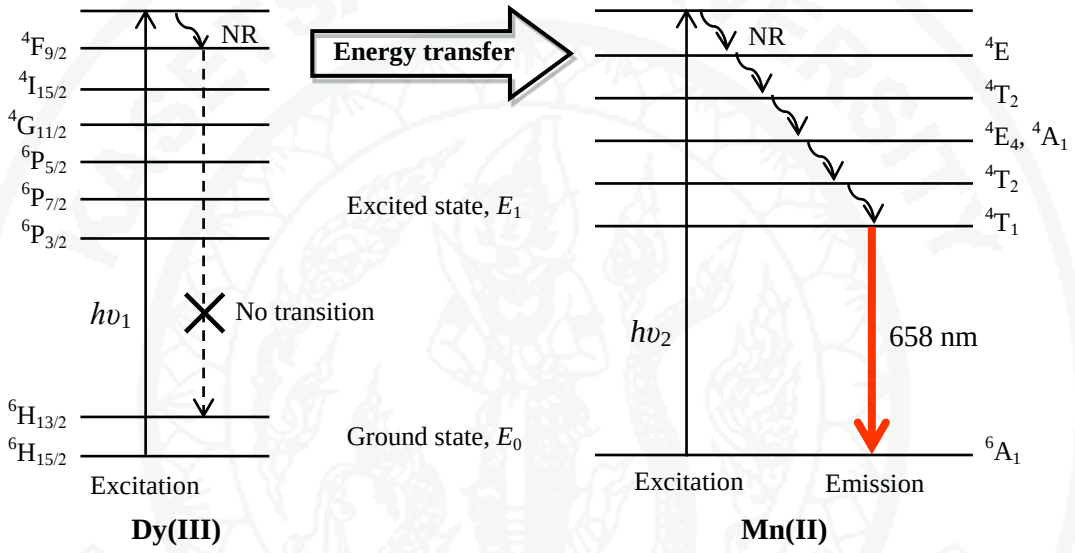

Figure 29 Schematic energy-level diagram showing the Dy(III)→Mn(II) energy transfer in co-doped $MgAl_2O_4$:Dy(III),Mn(II) ceramics.

The colored fluorescence of Dy(III),Mn(II)-codoped ceramics is an effect of the combined emission of Dy(III) and Mn(II) phosphors. The appearing color is likely to vary according to the fluorescence intensity of Dy(III) at 574.5 nm, and of Mn(II) at 658 nm. Thus, the appeared color of the fluorescence from Dy(III),Mn(II)-codoped ceramics may be altered or modified by varying the amounts of the sensitizer Dy(III) and the activator Mn(II) — that is to adjust the fluorescence intensity ratio of Dy(III) and Mn(II).

CONCLUSION

Four different types of ceramics, *i.e.* undoped $MgAl_2O_4$ spinel, Dy(III)-doped, Mn(II)-doped, and Dy(III),Mn(II)-codoped $MgAl_2O_4$ ceramics, had been prepared by a method adapted from the process of oxide one-pot synthesis (OOPS) and stepwise calcination at low temperatures. The proposed method has the advantages of being simple and less energy consumption, in spite of the time consuming procedures. The precursors were synthesized in one-step reaction by mixing together the reacting materials, *i.e.* Al_2O_3 , MgO, triethanolamine, the dopant(s), and the solvent ethylene glycol, and heating the mixture at 190 °C for 6 h. The precursors were calcined in steps: 500 °C for 5 h, 750 °C for 5 h, and 850 °C for 2 h. The prolonging calcination, however, could not wholly transform the precursors to pure spinel. The produced ceramics were solid solution of γ-Al_2O_3 and $MgAl_2O_4$ as indicated by the XRD patterns. The microstructure of the ceramics, as revealed in the SEM images, were mostly blocky particles in irregular shapes with hexagonal crystalline form appeared occasionally. A fiber-like structure also occurred in the codoped ceramics.

The yellow fluorescence at 574.5 nm resulted from the $^4F_{9/2} \rightarrow {}^6H_{13/2}$ transition of Dy(III) suggests that Dy(III) ions enter the host lattice $MgAl_2O_4$ by replacing Mg(II) in the tetrahedral sites. The reddish-orange fluorescence at λ_{em} 658 nm, corresponding to the $^4T_1 \rightarrow {}^6A_1$ transition of Mn(II), indicates that Mn(II) ions replace Al(III) ions in the octahedral site of the $MgAl_2O_4$ lattice. Despite the incomplete transformation to pure $MgAl_2O_4$, the developed method was found to be effective for the spinel doping. The compositions of the synthesized ceramics, as determined by EDX, showed satisfactory doping yield of 99.26 ± 25.91 % at 95 %CL.

The fluorescence of Dy(III),Mn(II)-codoped ceramics was a combined emission of Dy(III) and Mn(II) phosphors. The fluorescence of Mn(II) in the codoped ceramics was also found to be intensified by the presence of Dy(III) owing to the energy transfer from Dy(III) to Mn(II). Thus, the appeared color and the fluorescence intensity of the codoped ceramics may be modified or altered by varying the amounts of the sensitizer Dy(III) and the activator Mn(II).

LITERATURE CITED

Ayvacıkli, M., Z. Kotan, E. Ekdal, Y. Karabulut, A. Canimoglu, J. Garcia Guinea, A. Khatab, M. Henini and N. Can. 2013 Solid state synthesis of $SrAl_2O_4:Mn^{2+}$ co-doped with Nd^{3+} phosphor and its optical properties. **J. Lumin.** 144: 128-132.

Barpandaa, P., S.K. Behera, P.K. Gupta, S.K. Pratihar and S. Bhattacharya. 2006 Chemically induced order disorder transition in magnesium aluminium spinel. **J. Eur. Ceram. Soc.** 26: 2603-2609.

Caldino, U., E. Alvarez, A. Speghini and M. Bettinelli. 2012 Cold and warm white light generation using $Zn(PO_3)_2$ glasses activated by Ce^{3+}, Dy^{3+} and Mn^{2+}. **J. Lumin.** 132: 2077-2081.

Diao, C.C. and C.F. Yang. 2010 Synthesis of high efficiency $Zn_2SiO_4:Mn^{2+}$ green phosphors using nano-particles. **Ceram. Int.** 36: 1653–1657.

Dong, Y., Z. Wu, X. Han, R. Chen and W. Gu. 2011 Preparation of $BaMgAl_{10}O_{17}:Eu^{2+}$ phosphor with small particle size by co-precipitation method. **J. Alloy. Compd.** 506: 3638–3643.

Gedam, S.C., S.J. Dhoble and S.V. Moharil. 2007 $Dy^{3+}$and Mn^{2+} emission in $KMgSO_4Cl$ phosphor. **J. Lumin.** 124: 120-126.

Gómez, I., M. Hernández, J. Aguilar and M. Hinojosa. 2004 Comparative study of microwave and conventional processing of $MgAl_2O_4$-based materials. **Ceram. Int.** 30: 893-900.

Guanghuan, L. Tao, S. Yanhua, G. Guimei, X. Jijing, A. Baichao, G. Shucai and H. Guangyan. 2010 Preparation and luminescent properties of $CaAl_2O_4:Eu^{3+},R^+$ (R=Li, Na, K) phosphors. **J. Rare Earth** 28 (1): 22-25.

Hara, S., Y. Yoshida, S. Ikeda, N. Shirakawa, M.K. Crawford, K. Takase, Y. Takano and K. Sekizawa. 2005 Crystal growth of germanium-basedoxide spinels by the float zone method. **J. Cryst. Growth** 283: 185–192.

Karabulut, Y., A. Canimoglu, Z. Kotan, O. Akyuz and E. Ekdal. 2014 Luminescence of dysprosium doped strontium aluminate phosphors by codoping with manganese ion. **J. Alloy. Compd.** 583: 91-95.

Katsumata, T., T. Nabae, K. Sasajima and T. Matsuzawa. 1998 Growth and characteristics of long persistent $SrA1_2O_4$- and $CaAl_2O_4$-based phosphor crystals by a floating zone technique. **J. Cryst. Growth.** 1998. 183: 361-365.

Kawano, M., H. Takebe and M. Kuwabara. 2009 Compositional dependence of the luminescence properties of Mn^{2+}-doped metaphosphate glasses. **Opt. Mater.** 32: 277-280.

Kijjanukij, S. 2006. **Preparation and characterization of $MgAl_2O_4$ ceramic via Sol-gel process.** M.S. Thesis. Kasetsart University.

Lai, H., A. Bao, Y. Yang, W. Xu, Y. Tao and H. Yang. 2008 Preparation and luminescence property of Dy^{3+}-doped YPO_4 phosphors. **J. Lumin.** 128: 521-524.

Lakshmanan, A.R. 1999 Photoluminescence and thermostimulated luminescence processes in rare-earth-doped $CaSO_4$ phosphors. **Prog. Mater. Sci.** 44: 1-187.

Lakshminarayana, G. and L. Wondraczek. 2011 Photoluminescence and energy transfer in Tb^{3+}/Mn^{2+} co-doped $ZnAl_2O_4$ glass ceramics. **J. Solid State Chem.** 184: 1931-1938.

Laobuthee, A., S. Wongkasemjit, E. Traversa and R. Laine. 2000 $MgAl_2O_4$ spinel powders from oxide one pot synthesis (OOPS) process for ceramic humidity sensors. **J. Eur. Ceram. Soc.** 20: 91-97.

Lei, F. and B. Yan. 2008 Hydrothermal synthesis and luminescence of $CaMO_4:RE^{3+}$ (*M* = W, Mo; *RE* = Eu, Tb) submicro-phosphors. **J. Solid State Chem.** 181: 855-862.

Maia, A.S., R. Stefani, C.A. Kodaira, M.C.F.C. Felinto, E.E.S. Teotonio and H.F. Brito. 2008 Luminescent nanoparticles of $MgAl_2O_4$:Eu,Dy prepared by citrate sol–gel method. **Opt. Mater.** 31: 440-444.

Norris, D.J., N. Yao, F.T. Charnock and T.A. Kennedy. 2001 High-quality manganese-doped ZnSe nanocrystals. **Nano. Lett.** 1: 3–7.

Omkaram, I., and S. Buddhudu. 2009 Photoluminescence properties of $MgAl_2O_4:Dy^{3+}$ powder phosphor. **Opt. Mater.** 32: 8-11.

Palumbo, D.T. and J.J. Brown. 1970 Electronic states of Mn^{2+} activated phosphors. **J. Electrochem. Soc.** 117: 1184–1188.

Shinoya, S. and W.M. Yen. 1999. **Phosphor handbook**, CRC Press, Florida, United States of America.

Sohn, K.S., B. Cho and H.D. Park. 1999 Photoluminescence behavior of manganese-doped zinc silicate phosphors. **J. Am. Ceram. Soc.** 82: 2779-2784.

Tanabe, Y. and S. Sugano. 1954 On the absorption spectra of complex ions I. **J. Phys. Soc. Jpn.** 9 (5): 753-766.

Tomita A., T. Sato, K. Tanaka, Y. Kawabe, M. Shirai, K. Tanaka and E. Hanamura. 2004 Luminescence channels of manganese-doped spinel. **J. Lumin.** 109: 19-24.

Tong, Y.H., F. Cao, J.T. Yang, P.S. Tang and M.H. Xu. 2013 Intra-manganese luminescence in ZnO:Mn^{2+} nanorods prepared by a simple thermal evaporation process. **Mater. Lett.** 94: 124-127.

Ummartyotin, S., N. Bunnak, J. Juntaro, M. Sain and H. Manuspiya. 2012 Synthesis and luminescence properties of ZnS and metal (Mn, Cu)-doped-ZnS ceramic powder. **Solid State Sci.** 14: 299-304.

Vijay, S., R.P.S. Chakradharb, J.L. Raoc and D. Kim. 2007 Synthesis, characterization, photoluminescence and EPR investigations of Mn doped $MgAl_2O_4$ phosphors. **J Solid State Chem.** 180: 2067-2074

Waldner, K. F., R. Laine, S. Dhumrongvaraporn, S. Tayaniphan and R. Narayanan. 1996 Synthesis of a double alkoxide precursor to spinel ($MgAl_2O_4$) directly from $Al(OH)_3$, MgO, and triethanolamine and its pyrolytic transformation to spinel. **Chem. Mater.** 8: 2850-2857.

Wu, G.S., Y.L. Zhuang, Z.Q. Lin, X.Y. Yuan, T. Xie and L.D. Zhang 2006 Synthesis and photoluminescence of Dy-doped ZnO nanowires. **Physica E** 31: 5–8.

Yan, B., H. Zhang, S. Wang, and J. Ni. 1998 Luminescence properties of rare-earth (Eu^{3+} and Tb^{3+}) complexes with paraaminobenzoic acid and 1,10-phenanthroline incorperated into a silica matrix by Sol-gel method. **Mater. Res. Bull.** 33 (10): 1517-1525.

Yao, G.Q., L. Zhang and M.Z. Sum 1997 Luminescence and energy transfer of Eu^{2+}, Mn^{2+} in $CaZn_2(PO_4)_2$. **Chem. J. Chin. Univ.** 18: 1–5.

Yong, G., C. Shi and Y. Wu. 1996 Luminescence properties of SrB_4O_7: Eu, Tb phosphors. **Mater. Res. Bull.** 31 (5): 439-444.

Yu, M., J. Lin, Z. Zhang, J. Fu, S. Wang, H.J. Zhang and Y.C. Ham. 2002 Fabrication, patterning and optical properties of nanocrystalline YVO_4:A (Eu^{3+}, Dy^{3+}, Sm^{3+}, Er^{3+}) Phosphor Films via Sol-Gel Soft Lithography. **Chem. Mater.** 14: 2224-2231.

Zhang, X., F. Meng, W. Li, S.I. Kim, Y.M. Yu and H.J. Seo. 2013 Investigation of energy transfer and concentration quenching of Dy^{3+} luminescence in $Gd(BO_2)_3$ by means of fluorescence dynamics. **J. Alloy. Compd.** 578: 72-76.

Zhihua L., Z. Jinghui, Z. Guochun and L. Yadong. 2005 A new promising phosphor, $Na_3La_2(BO_3)_3$:*Ln* (*Ln* = Eu, Tb). **J. Solid State Chem.** 178: 3624–3630.

APPENDIX

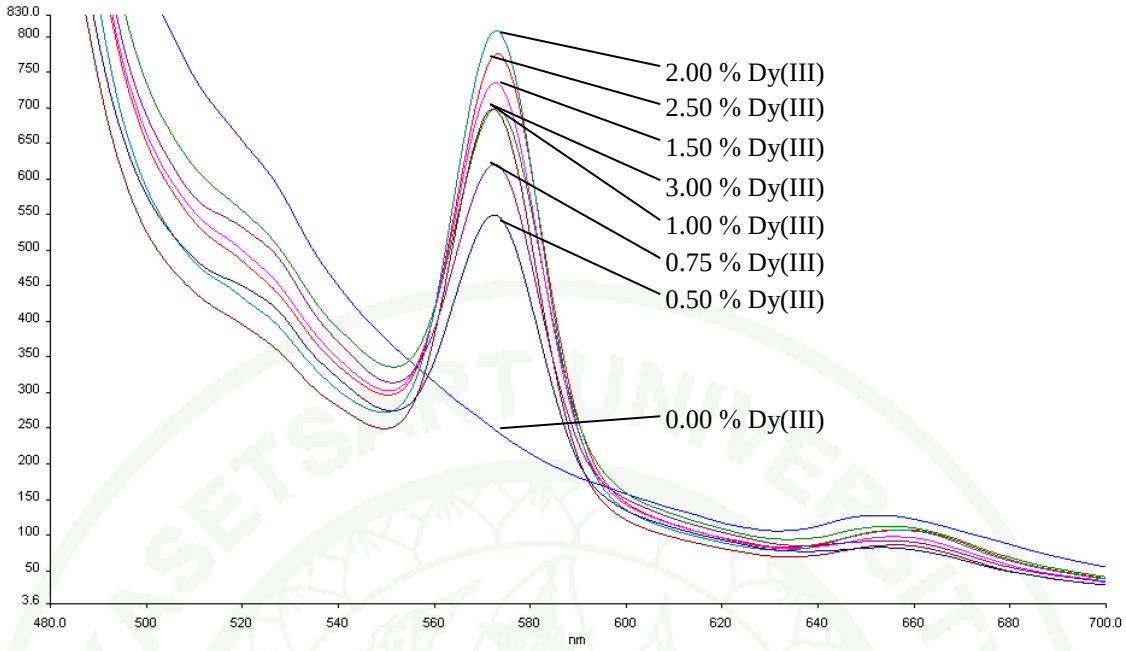

Appendix Figure 1 Emission spectra of Dy(III)-doped $MgAl_2O_4$ with various concentration of Dy(III)

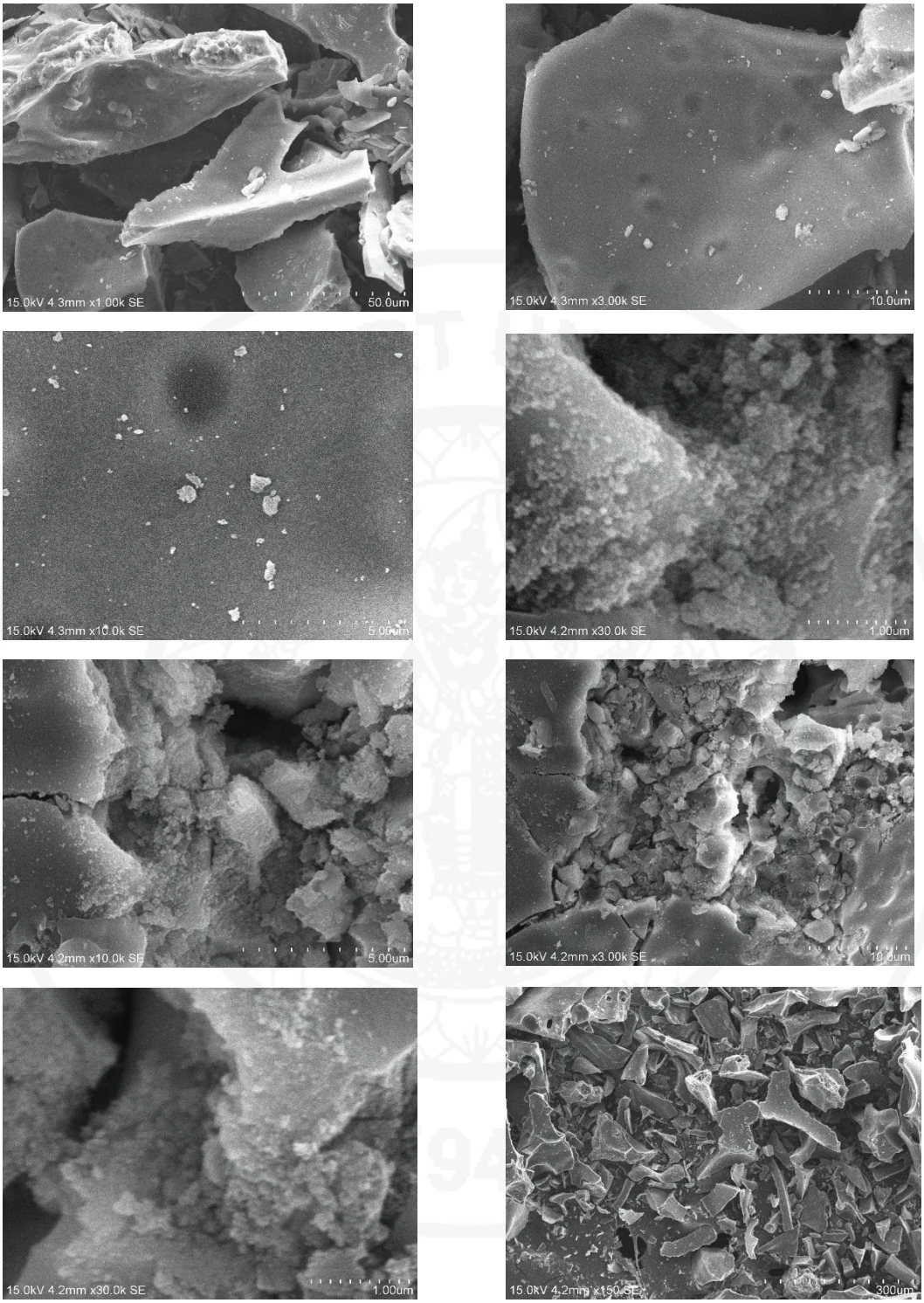

Appendix Figure 2 SEM images of $MgAl_2O_4$

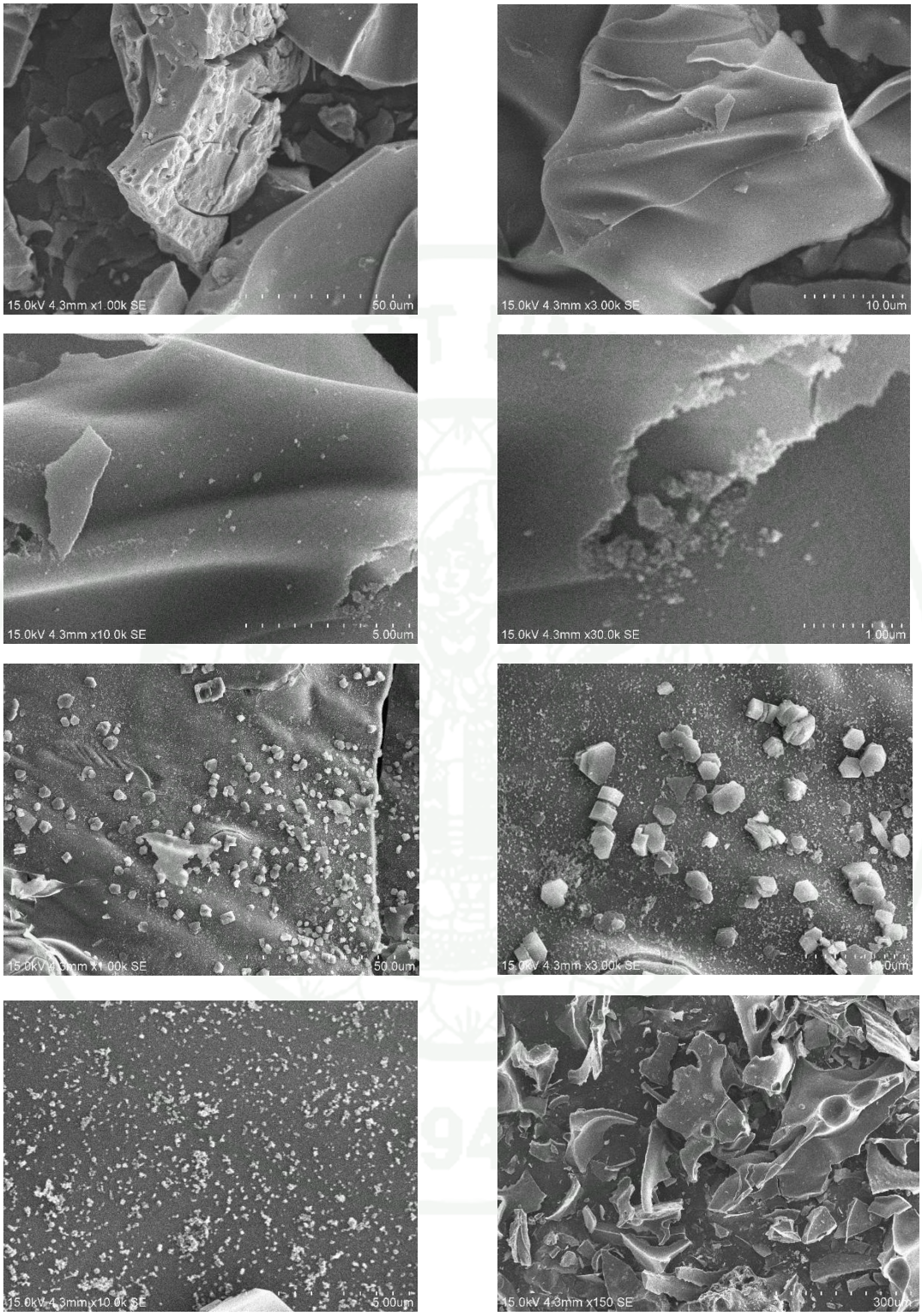

Appendix Figure 3 SEM images of 1%Dy(III)-doped $MgAl_2O_4$

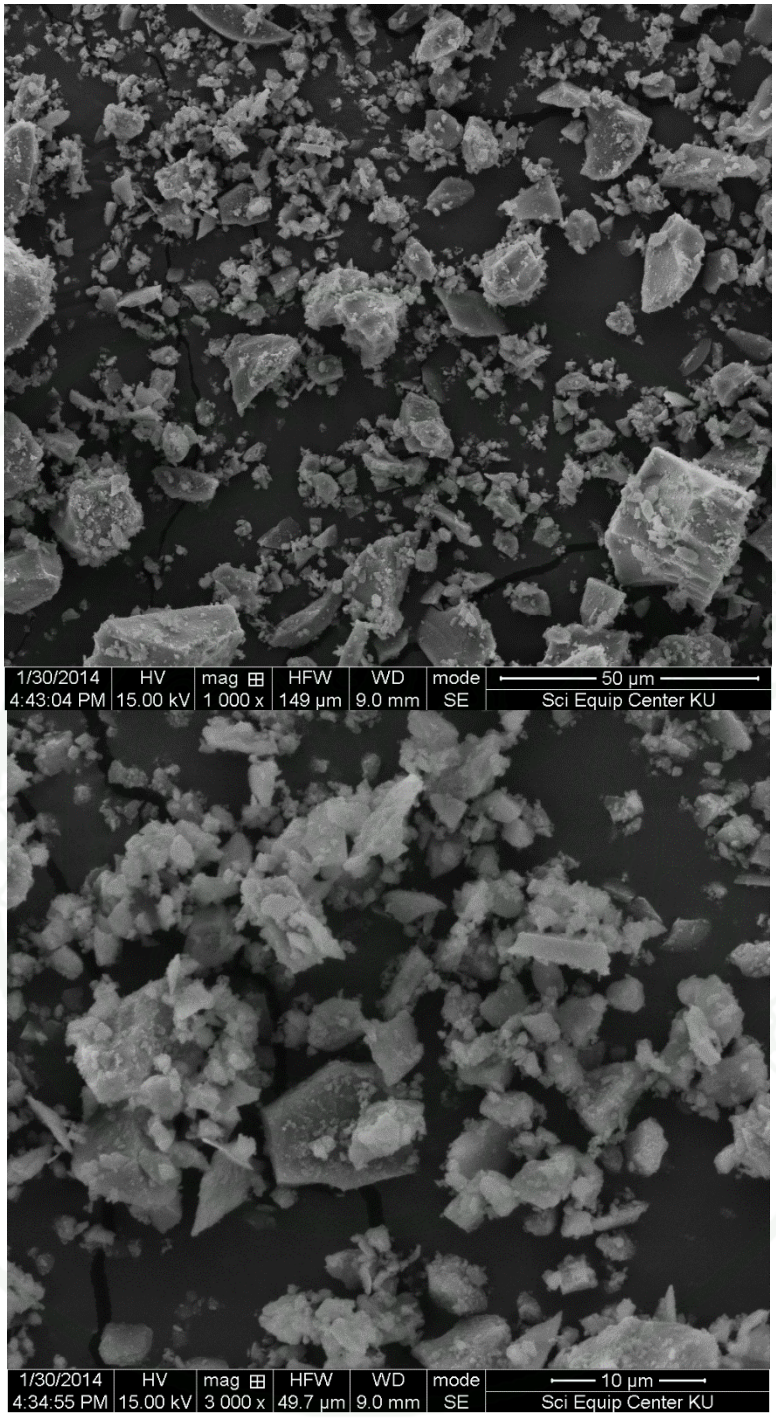

Appendix Figure 4 SEM images of 3%Dy(III)-doped $MgAl_2O_4$

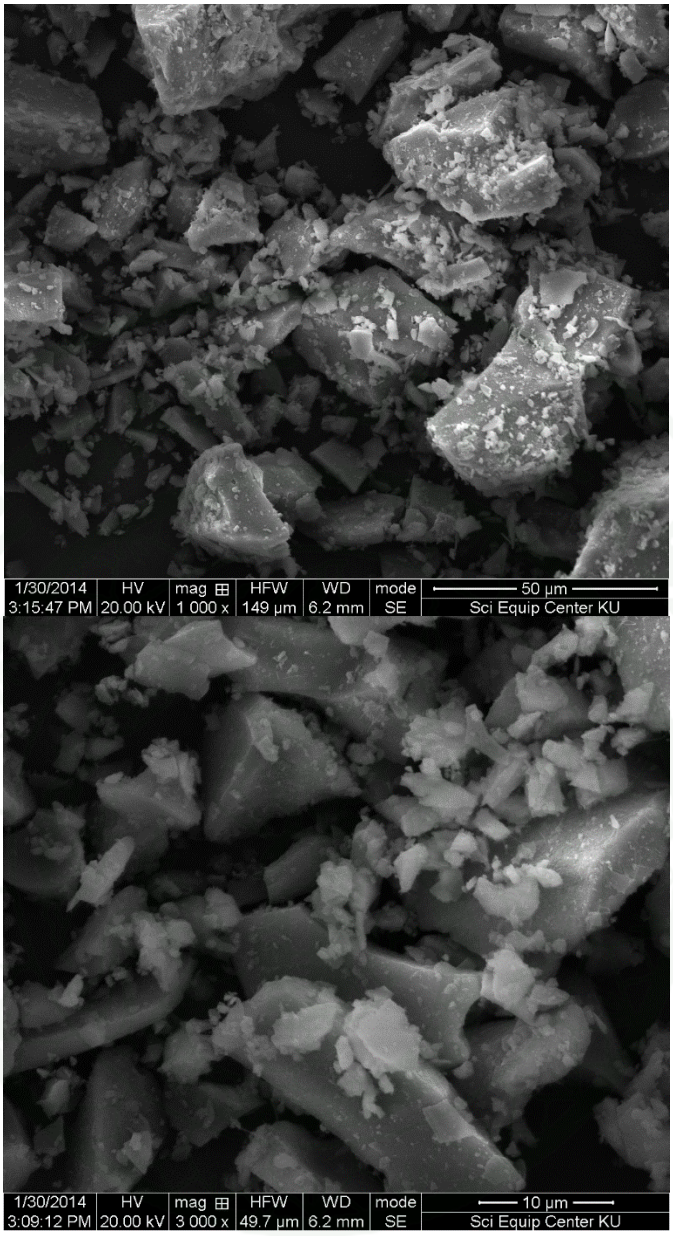

Appendix Figure 5 SEM images of 0.50% Mn-doped $MgAl_2O_4$

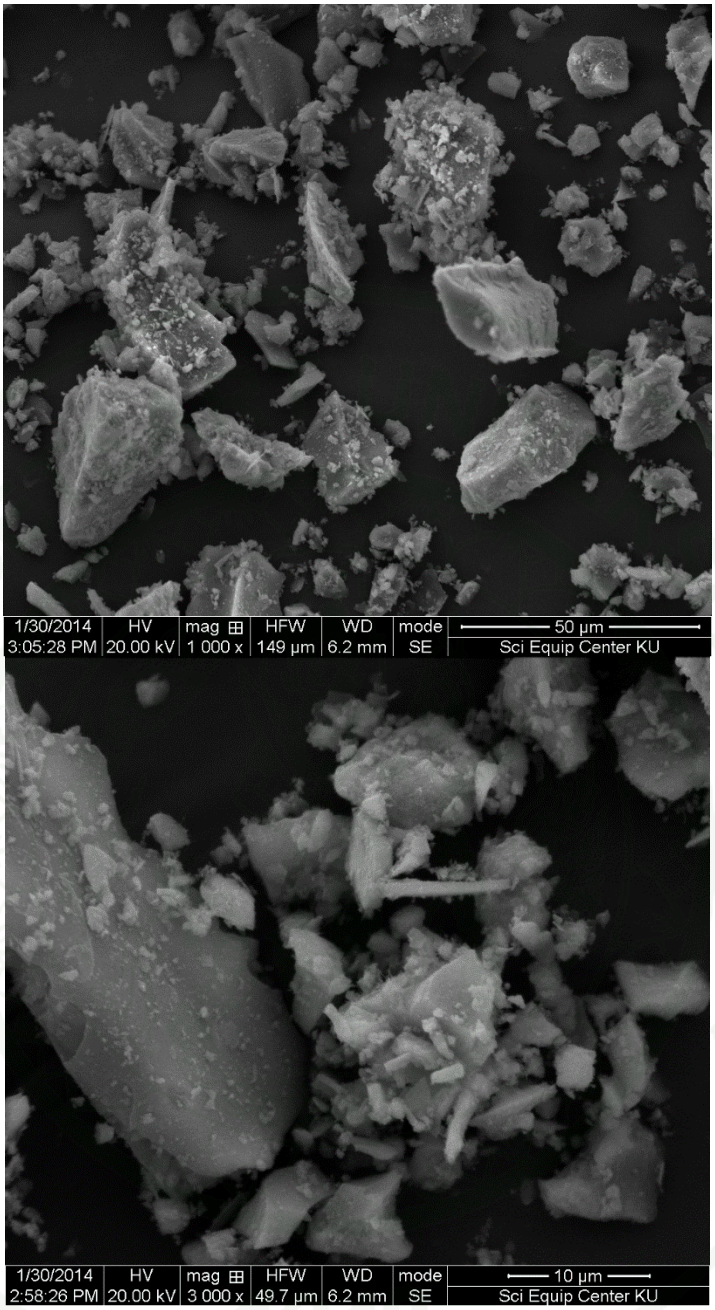

Appendix Figure 6 SEM images of 0.75%Mn(II)-doped $MgAl_2O_4$

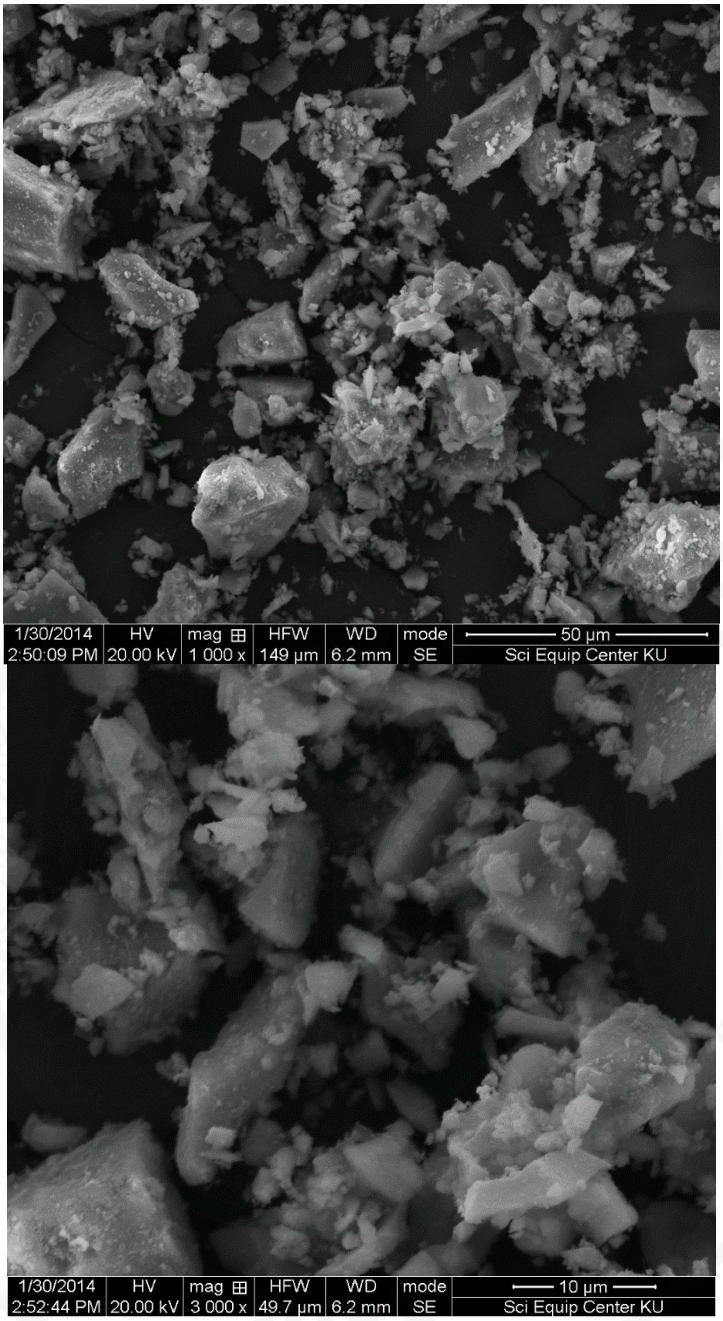

Appendix Figure 7 SEM images of 1.00%Mn(II)-doped $MgAl_2O_4$

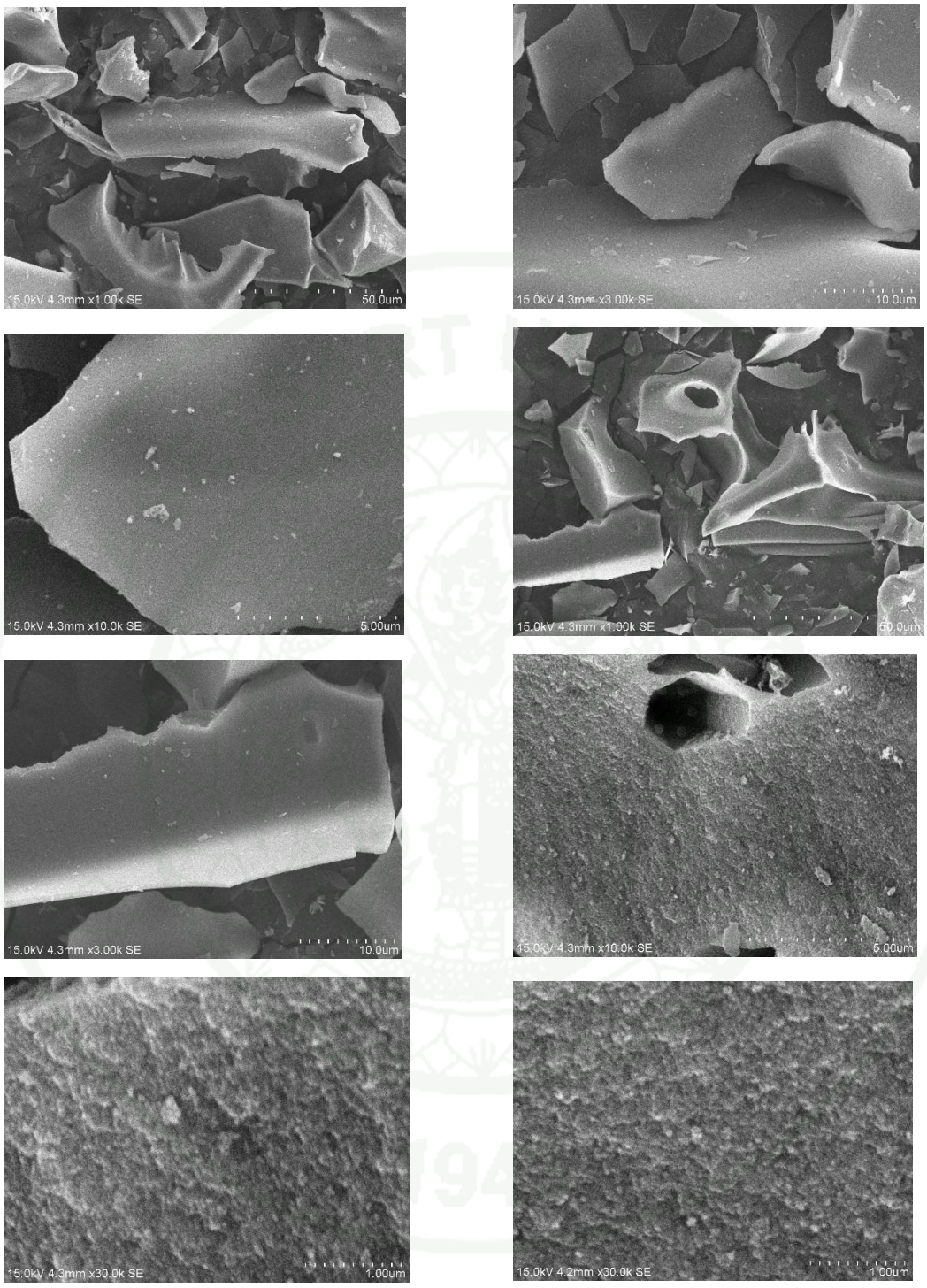

Appendix Figure 8 SEM images of 1.00% Mn(II)-doped $MgAl_2O_4$

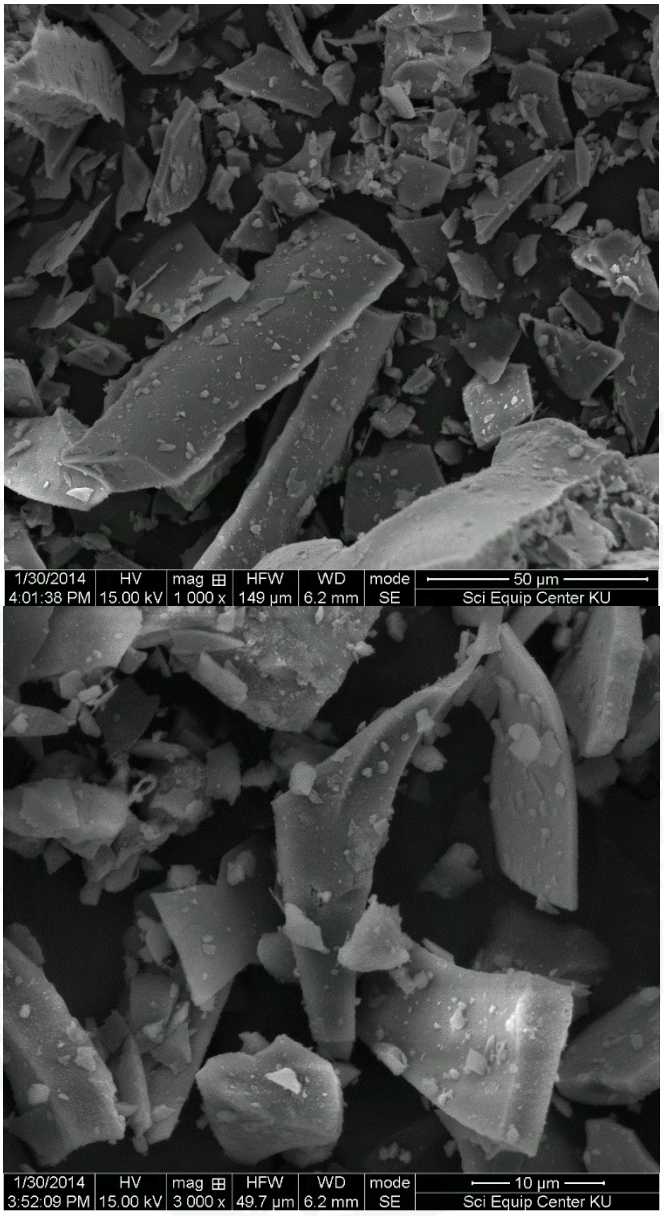

Appendix Figure 9 SEM images of 0.10% Mn(II), 1.00% Dy(III)-doped $MgAl_2O_4$

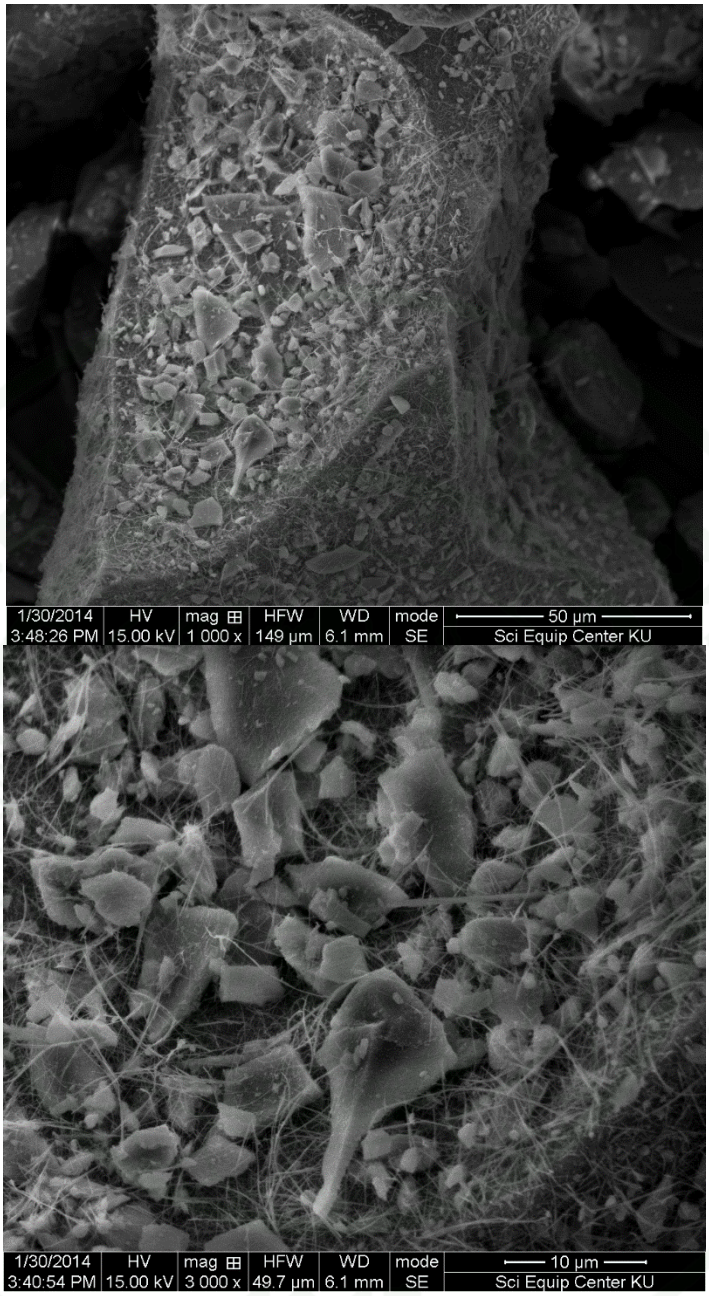

Appendix Figure 10 SEM images of 0.5% Mn, 1%Dy-doped $MgAl_2O_4$

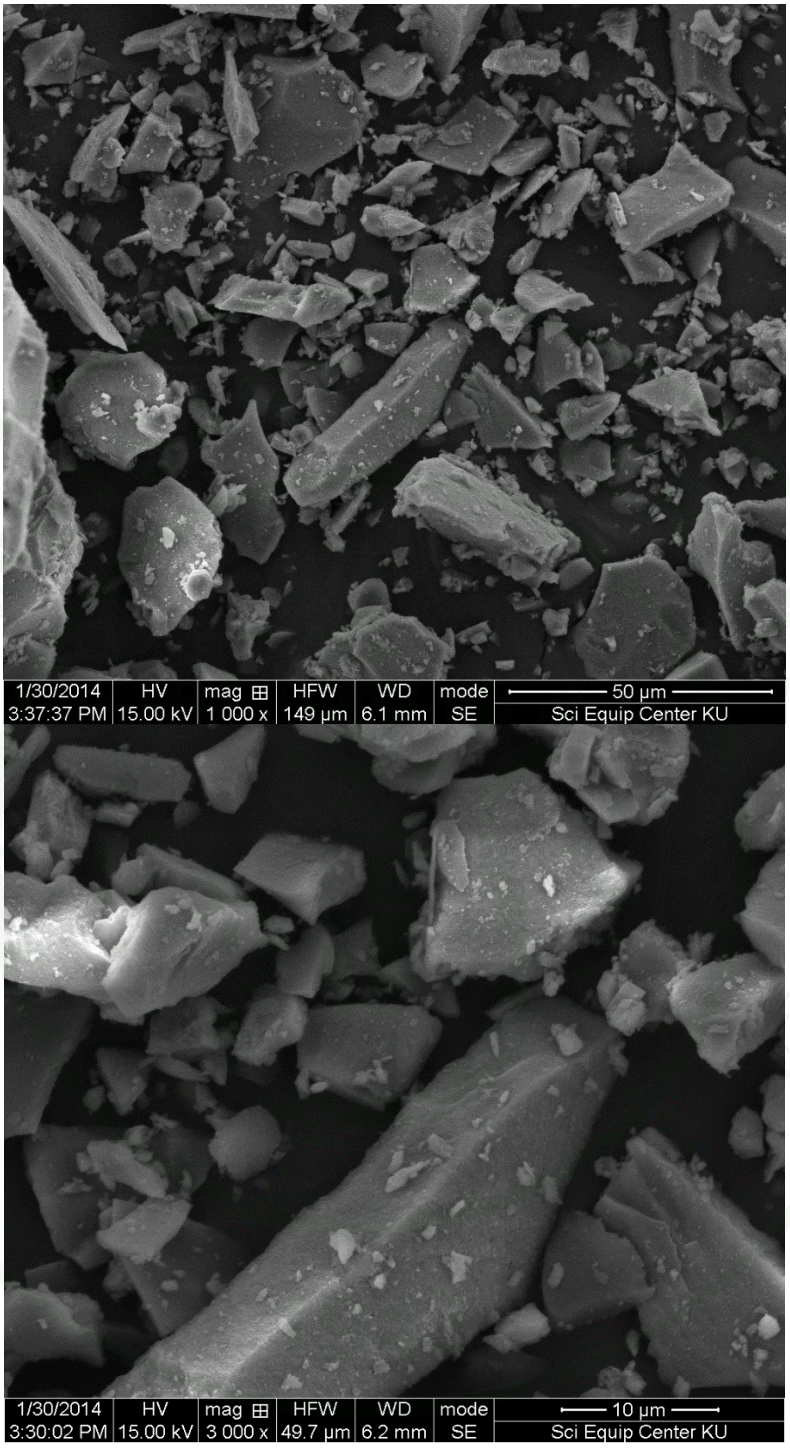

Appendix Figure 11 SEM images of 0.75% Mn(II), 1%Dy(III)-doped $MgAl_2O_4$

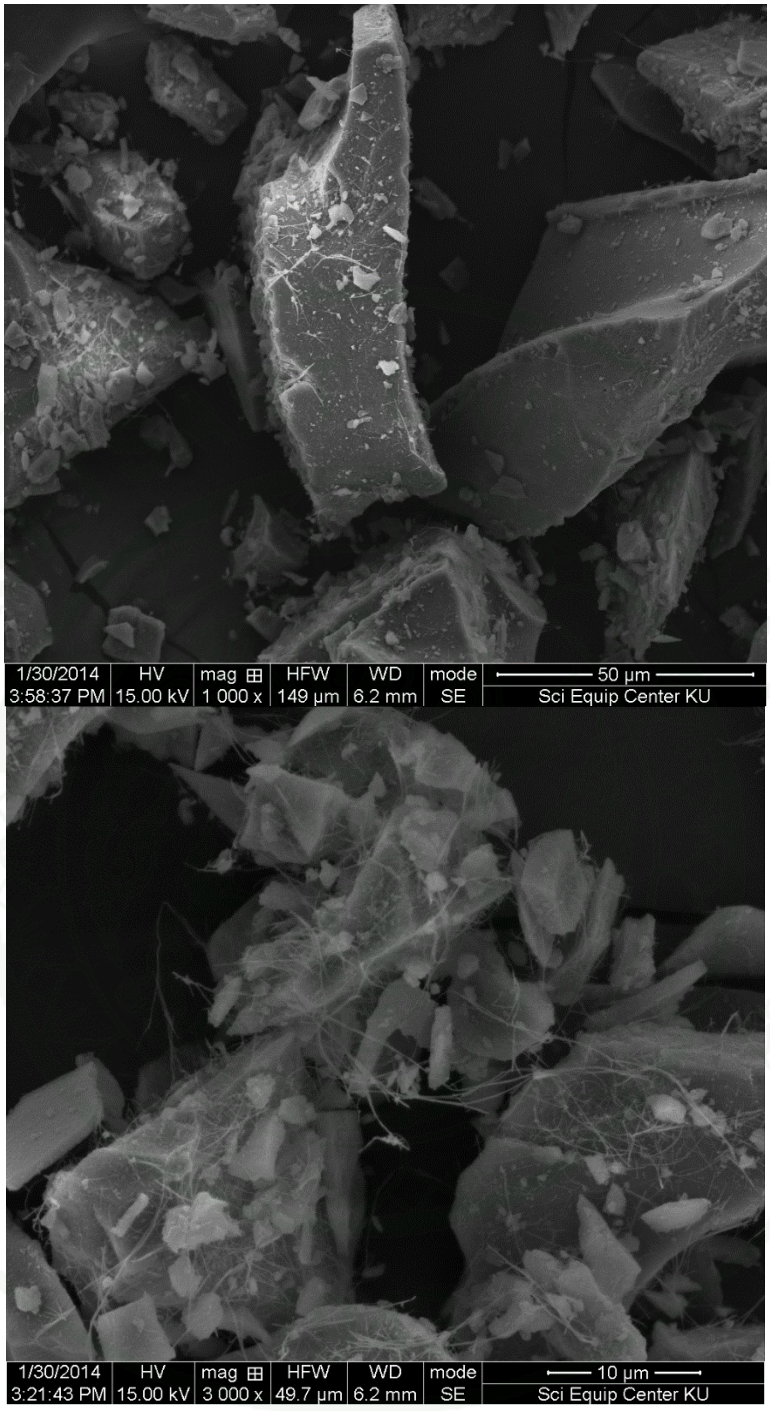

Appendix Figure 12 SEM images of 1.00% Mn(II), 1.00%Dy(III)-doped $MgAl_2O_4$

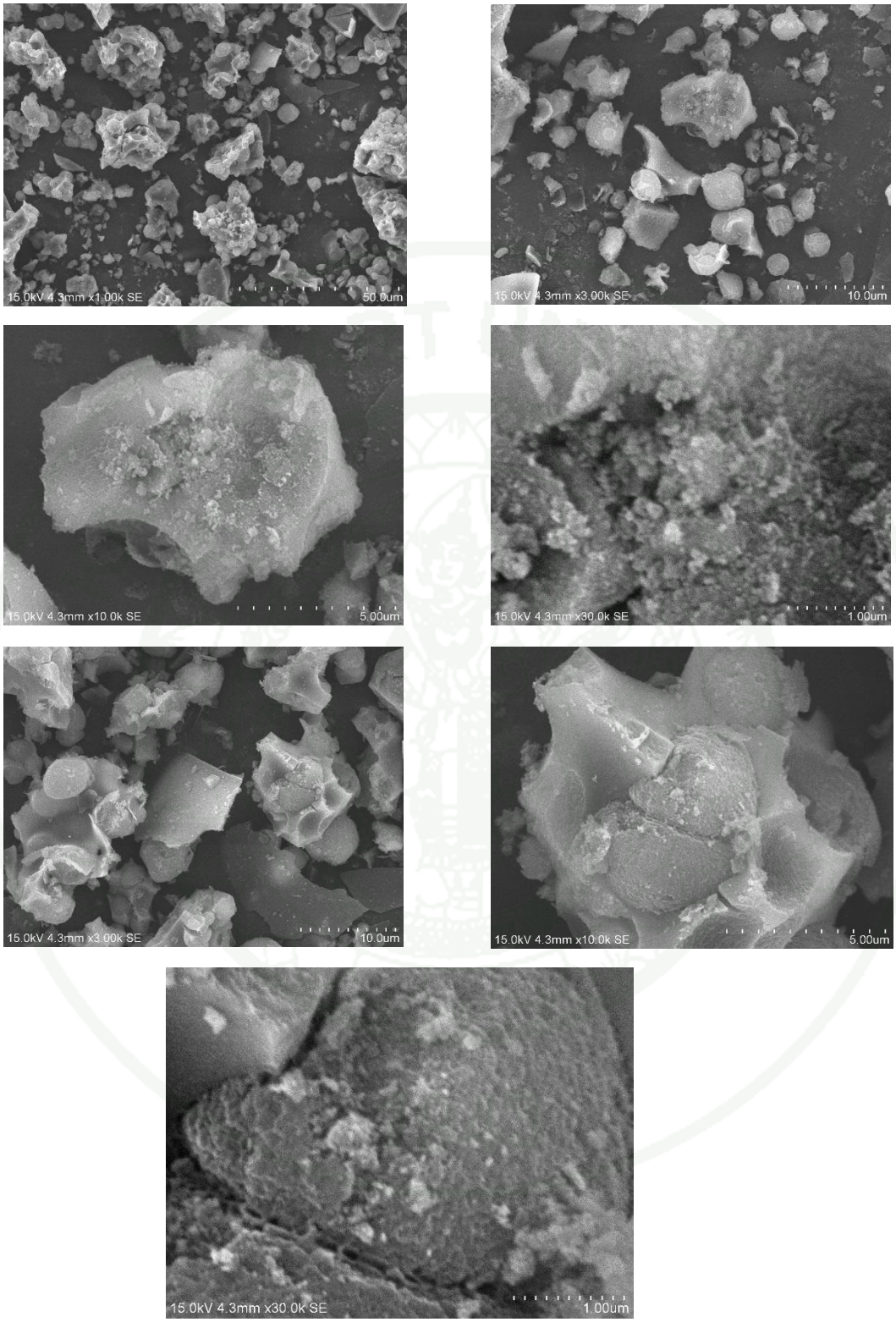

Appendix Figure 13 SEM images of 0.50% Mn(II), 0.50%Dy(III)-doped $MgAl_2O_4$

CIRRICULUM VITAE

NAME : Mr. Watnatee Pullarp

BIRTH DATE : March 8th, 1986

BIRTH PLACE : Bangkok, Thailand

EDUCATION :

YEAR	**INSTITUTE**	**DEGREE/DIPLOMA**
2009	Kasetsart Univ.	B.Sc. (Chemistry)

POSITION/TITLE : Postgraduate student

WORKPLACE : Faculty of Science, Kasetsart University

SCHOLARSHIP/AWARDS : -